Mechanism and Machine Theory 156 (2021) 104138

Contents lists available at ScienceDirect

Mechanism and Machine Theory

journal homepage: www.elsevier.com/locate/mechmachtheory

Leg design for biped locomotion with mono-articular and bi-articular linear actuation

Christine Chevallereau[a], Philippe Wenger[a,*], Yannick Aoustin[b], Franck Mercier[c], Nicolas Delanoue[c], Philippe Lucidarme[c]

[a] Centre National de la Recherche Scientifique, Laboratoire des Sciences du Numérique de Nantes (LS2N), UMR CNRS 6004, Nantes 44321, France
[b] Université de Nantes Laboratoire des Sciences du Numérique de Nantes (LS2N), UMR CNRS 6004, Nantes 44321, France
[c] Université d'Angers Laboratoire Angevin de Recherche en Ingénierie des Systèmes, Angers, France

ARTICLE INFO

Article history:
Received 16 July 2020
Revised 8 October 2020
Accepted 8 October 2020
Available online 21 October 2020

Keywords:
Biped leg
Optimal design
Linear motor
Mono-articular
Bi-articular
Energy

ABSTRACT

Implementing efficient actuators with good backdriveability properties is of primary importance for the design of high-performance performance bipedal robots. Nowadays, the use of linear direct drive electric motors is an interesting choice. This actuation scheme is closer to the efficient muscular system of human legs. However, the efficiency of linear motors is highly sensitive to the placement of their attachment points. Two main issues are addressed in this paper; (i) the optimal placement of the motors on the leg and (ii) the best actuation scheme of the leg with three motors when considering both mono-articular and bi-articular motors. Little research work has been devoted to these issues. Accordingly, a methodology is proposed to optimize linear motors attachment points. Instead of resorting to a pure numerical optimization, a first analytic-heuristic approach is proposed in order to obtain more insight into the optimization problem. This first approach, in addition to providing useful information, allows obtaining a good initial guess for the numerical optimization. Eventually, eight different leg architectures with three motors and combining different numbers of mono-articular and bi-articular motors are optimized. Results show the interest of using bi-articular motors to reduce the maximum effort required for each motor.

1. Introduction

Biped motions such as walking, running and jumping require a great amount of work from motors [1,2]. They must produce forces experiencing drastic magnitude changes over time according to the different movement phases. These forces also strongly depend on the robot parameters as well as on the environment. Moreover, an important need to be considered in the design of bipeds is to absorb the effects of high impacts with the ground. Selecting an appropriate leg architecture and choosing suitable motors is therefore of primary importance, especially since they generally represent nearly 40% of the

* Corresponding author.
E-mail addresses: christine.chevallereau@ls2n.fr (C. Chevallereau), philippe.wenger@ls2n.fr, philippe.wenger@irccyn.ec-nantes.fr (P. Wenger), yannick.aoustin@univ-nantes.fr (Y. Aoustin), franck.mercier@univ-angers.fr (F. Mercier), nicolas.delanoue@univ-angers.fr (N. Delanoue), philippe.lucidarme@univ-angers.fr (P. Lucidarme).

https://doi.org/10.1016/j.mechmachtheory.2020.104138
0094-114X/

total mass of the biped [3]. Two main types of motors can be used to actuate the legs of a biped, namely, rotary motors and linear motors.

1.1. Backdriveability and rotary motors

Backdriveability is an interesting feature that offers a natural low impedance [4,5] and allow cushioning shocks. A metric named "impact mitigation factor" (IMF) to quantify backdrivability is proposed in [6]. Rotary motors are often used in current biped designs, because their technology is well known and they may allow unlimited joint rotations. Rotary motors are most often equipped with reduction gears in order to achieve sufficient torque. Sellaouti et al. [7] designed a three-degree-of-freedom parallel mechanism to actuate the hip and the ankle joints of their ROBIAN biped. Omer et al. [8] proposed a mechanism called bi-directional adjustable stiffness artificial tendon (BIASAT) for the ankle pitch joint of WABIAN-2R in order to provide passive and active motions. However, rotary motors have some drawbacks, such as the presence of dynamic imbalance in the frontal plane when the output axis is not aligned with the articulated bodies, and the lack of backdriveability when a reduction device is necessary to increase the torque. The absence of backdriveability in rotary motors with reduction gears can be compensated by the use of *SEA* (Selective Elastic Actuator). They can passively conform to unmodeled disturbances [9]. Sharbafi et al. [10] present three bio-inspired legged robots with leg musculoskeletal architectures similar to humans, *BioBiped1, BioBiped2*, and *BioBiped3*. They used compliant musculoskeletal bipedal systems with SEA to mimic biological muscles. However, SEA suffer from a number of shortcomings, such as limitations on actuation bandwidth and introduction of control complexities [11,12]. Backdriveability can also be available by adding a variable stiffness mechanism to a rotary motor. Such a solution was used in the design of exoskeletons [13]. Compliantly actuated legs with both series and parallel-elastic actuation have also been proposed for bipeds [14] or wearable robot [15]. Another way to allow backdriveability is to use direct drive (DD) motors. Rotative DD motors have been used in several legged robots, see [11,16,17] for example. However, the limited torque capability of these motors reduces the scope of their use to low-demanding applications. In many cases, a low-ratio gearbox or planetary gear must be embedded to improve the balance between motor size, backdrivability, bandwidth and output torque [6,11,18]. Rotative DD motors are also often space consuming. Previous work on the MIT Cheetah robot has shown that building a full size quadruped robot requires at least 76 cm DD rotary motors [6].

1.2. Backdriveability and linear motors

Linear motors are easier to embed in body segments spaces than rotary motors in joints. Three types of backdriveable linear motors can be considered for a legged robot, (i) electric DD motors, (ii) pneumatic motors and (iii) hydraulic motors. Pneumatic motors have been experimented with some interesting results, such as in the Pneupard biomimetic quadruped robot [19]. Unfortunately, the use of compressors is an obstacle for embedded systems. Hydraulic motors were implemented in the famous BigDog from Boston Dynamics. Well known for its performance in rough terrain, BigDog embedded a 15 hp combustion engine that drives a pump delivering high-pressure hydraulic oil to the robot's leg actuators [20]. This architecture, shared with the Atlas robot [21], is heavy to implement, noisy and expensive. When compared to pneumatic and hydraulic motors, electric DD motors have better dynamic properties and simple direct output force control capabilities [22]. With a six-quadrant driver, linear DD motors can be used as generators to break the acceleration during a downhill walking phase and thus store energy for later use [23]. Electric linear motors have been used to build exoskeletons [24] or bipeds using parallel mechanisms to model contribution of several muscles [25–27]. In [28], the authors have developed a customized linear DD motor to be used in a cheetah leg. Several efficient electric linear DD motors have appeared recently on the market. Designed on the basis of [29], these motors can produce high peak forces at extremely high accelerations and speeds. Their prime asset relies on high backdrivability. In summary, electric linear motors appear as good candidates to design biped robots with high performance and backdriveability properties.

1.3. Design methodology for the placement of linear motors

Linear motors are connected to the limbs and apply forces on the joints, like muscles. In humans and animals, mono and bi-articular muscles coexist [30–32] and have their own interests [14,33–35]. Thus, both mono and bi-articular motors can be considered in the design of a biped's leg. One drawback of linear motors is the occurrence of a singularity when the slider axis meets the joint axis. In this configuration, no torque can be transmitted. Thus, a special attention must be paid to the positioning of the motor on the bipedal structure. Expected designs must be far enough from singularities and produce sufficient torque on the desired rotation range of all joints. The solution to this problem is tackled at the geometric design level by optimizing the attachment points of the linear motors on the leg structure. Since the torque produced by the linear motor at a joint depends on the robot configuration, the design process must be based on expected motions of the prototype.

It is worth noting that little research has been devoted to this issue. To the best of the authors' knowledge, the only contribution to this problem is a generic approach proposed by Ha et al. [36]. They provide a general algorithm for optimizing robot parameters of manipulators or legged robots. Upon linearizing the manifold of valid parameters implicitly defined by constraints, the algorithm allows tuning some of the design or motion parameters while remaining on the aforementioned

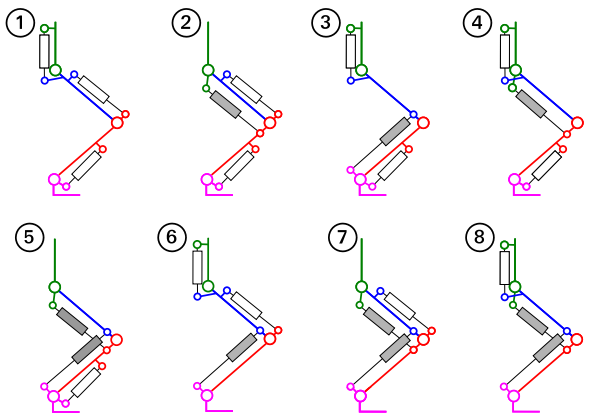

Fig. 1. The eight possible actuation schemes for one robot leg. The two attachment points of any mono-articular (resp. bi-articular) motor are separated by one (resp. two) joints. Attachment points are depicted with the same color as their respective anchor body. For instance, the blue upper (resp. red lower) attachment point of the mono-articular knee motor in the first architecture (M_a, M_k, M_h) is linked to the femur (resp. tibia). Mono-articular (resp. bi-articular) motors are shown in white (resp. grey) rectangles. (For interpretation of the references to color in this figure legend, the reader is referred to the web version of this article.)

manifold. Their algorithm applies to the design of robots with both rotary and linear DD motors. However, since their approach is generic and operates locally, it is hard to appreciate the quality of the optimal solution. Seok et al. [18] present design principles for developing energy-efficient legged robots. Energy loss is analyzed through the entire system but no design methodology is provided for optimizing the geometric parameters.

From the literature review, in conclusion, there is no specific, well-designed strategy to find suitable placements of the attachment points of linear motors with an optimal lever arm and allowing a human-like walking. Accordingly, this paper proposes an original strategy based on an optimization algorithm for a biped robot when each leg is actuated by three linear motors. Most existing design methodologies rely on dynamic simulations and require time-consuming iterative processes without guarantee of optimality [36,37]. Contrary to previous work, the method in this paper is based on the kinematic model relating joint torques and motor forces.

Human legs are actuated with a set of antagonistic pulling muscles. Since linear motors can both pull and push, they can replace a set of antagonistic muscles. In human legs, many groups of muscles produce redundant actuation, but this work is limited to the use of non-redundant actuation schemes with only three motors per leg in sagittal plane. The following main issues are tackled in this paper:

- What are the best attachment points of the motors, for a given architecture?
- What is the best actuation architecture with three motors?

Eight leg architectures, shown in Fig. 1, combining mono-articular and bi-articular motors are investigated for walking and squat motions. As a result of our numerical tests, we show that the best design for the desired trajectories is a leg architecture combining two bi-articular motors ankle-knee and knee-hip along with a mono-articular motor at the ankle.

This paper is organized as follows. Section 2 presents the dynamic model and the contribution of motor forces to this model. The statement of the problem is defined in Section 3. The optimal placement of the motor attachment points is defined for mono-articular motors in Section 4. Two successive approaches are used: an analytic-heuristic approach and a numerical optimization. The extension to an optimal design including bi-articular motors is discussed in Section 5. The eight proposed leg architectures for a planar biped with three motors per leg are optimized and the results are discussed in Section 6. Last section concludes this paper.

2. Dynamic model of mechanical structure

2.1. Notations and preliminary information

A mono-articular linear motor actuates only one joint. Besides, its two attachment points are located on each side of the actuated joint. On the contrary, a bi-articular linear motor actuates two joints and its two attachment points are separated by two successive joints. Based on biomimetic inspiration, we limit our study to mono-articular or bi-articular motors and do not consider multi-articular motors connecting the foot and the trunk. The following notations are used: M_h: mono-articular hip motor, M_{hk}: bi-articular hip knee motor, M_k: mono-articular knee motor, M_{ka}: bi-articular knee ankle motor and M_a: mono-articular ankle motor.

In order to build an anthropomorphic robot, predefined mass distribution and inertia are considered. Winter's parameters are used [37] to describe the robot bodies. The mass distribution is assumed identical for all studied actuation types whatever the choice of motors and their attachment points. Accordingly, we produce a preliminary design step. A detailed

Table 1
Main data of the planar biped studied.

Body	Mass kg	Length m	Inertia kg m^2
Trunk	42	0.81	2.57
Thigh	6.2	0.424	1.63
Calf	2.88	0.426	0.05
Foot	0.9	0.20	0.009

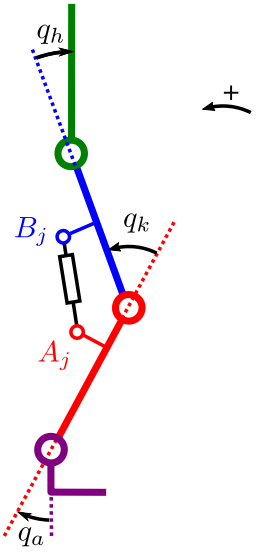

Fig. 2. Joint angles description (measured counter-clockwise).

design can be envisaged in a second step by taking into account bodies' mass and motors' mass separately. This second step is out of the scope of this paper. The main data of the four bodies modelled in sagittal plane are given in Table 1 for a human of height 1.72 m and weight of 62 kg. The height of the foot is 0.07 m.

2.2. Taking into account the mechanical structure

Each leg comprises four bodies associated with the foot, the calf, the thigh, and the trunk, respectively. The two legs are assumed to have the same design. In this context, the dynamic model can be written when the robot is assumed to be in support with one foot flat to the ground. The unilateral constraints between this stance foot and the ground are implicitly taken into account. The model can thus be written in Lagrange form as follows:

$$A(q)\ddot{q} + C(q,\dot{q})\dot{q} + G(q) = \Gamma, \tag{1}$$

where q is the vector of joint variables. For a planar biped robot, q normally contains the joint variables of the two legs, but since only one leg needs to be considered in this study, q can be reduced to any one leg. Then, q is written as $q = [q_a, q_k, q_h]^\top$, where q_a is the ankle angle (relative angle with respect to the perpendicular of the sole of the foot), q_k is the knee (relative) angle and q_h is the hip (relative) angle, see Fig. 2.

Since all motors are linear and not rotary, the vector of joint torques Γ does not contain the motor torques. In fact, it contains the moments applied by the linear motors on the joints. This vector can be derived from the virtual work of the motors. For the same reasons as above, vector Γ is restricted to any one leg. Moreover, $\Gamma = [\Gamma_a, \Gamma_k, \Gamma_h]^\top$, where the indices a, k, h stand for ankle, knee, and hip respectively.

2.3. Motor consideration

Let us denote A_j and B_j the distal and proximal attachment points of the linear motor j on the leg (see Fig. 2) and let F_j denote the force applied by the linear motor. The virtual work δW of the force of magnitude F_j for a virtual displacement $\delta\overrightarrow{A_jB_j}$ can be written as follows:

$$\delta W = F_j \frac{\overrightarrow{A_jB_j}}{\|\overrightarrow{A_jB_j}\|} \cdot \delta\overrightarrow{A_jB_j} \tag{2}$$

Points A_j and B_j are linked to the leg and their coordinates can therefore be written as functions of q. The right-hand side of Eq. (2) must be written as a function of the joint angles and of their virtual displacements. To do so, the case of mono-articular and bi-articular motors must be treated separately.

Let us first consider a mono-articular motor j placed around joint q_j, where j is a (ankle), k (knee) or h (hip). Then, $\overrightarrow{A_jB_j}$ (resp. $\delta\overrightarrow{A_jB_j}$) can be expressed as a function of q_j only (resp. δq_j). The virtual work can be written as:

$$\delta W = F_j J_{j,j}(q_j)\delta q_j. \tag{3}$$

and

$$\Gamma_j = J_{j,j}(q_j)F_j. \tag{4}$$

where $J_{j,j}(q_j)$ is a scalar expression detailed in Section 4.1. As shown in that section, $J_{j,j}(q_j)$ defines the lever arm, i.e. the distance between the action line of the linear motor and the center of the joint. This distance depends on q_j.

Let us now consider a bi-articular motor j spanning joints q_i and q_l, where i (resp. l) is either a or k (resp. k or h). Here, j is ak or kh. Then, $\overrightarrow{A_jB_j}$ and $\delta\overrightarrow{A_jB_j}$ can be written as functions of q_i and q_l. Accordingly, the virtual work can be expressed as follows:

$$\delta W = F_j\begin{bmatrix} J_{i,j}(q_i, q_l) & J_{l,j}(q_i, q_l)\end{bmatrix}\begin{bmatrix}\delta q_i \\ \delta q_l\end{bmatrix}. \tag{5}$$

In this case, the joint torques can be expressed as follows:

$$\begin{bmatrix}\Gamma_i \\ \Gamma_l\end{bmatrix} = \begin{bmatrix} J_{i,j}(q_i, q_l) \\ J_{l,j}(q_i, q_l)\end{bmatrix}F_j. \tag{6}$$

When all possible motors are considered, the following general model is obtained [38]:

$$\Gamma = J(q_a, q_k, q_h)F \tag{7}$$

or, in more details:

$$\begin{bmatrix}\Gamma_a \\ \Gamma_k \\ \Gamma_h\end{bmatrix} = \begin{bmatrix} J_{a,a} & J_{a,ak} & 0 & 0 & 0 \\ 0 & J_{k,ak} & J_{k,k} & J_{k,kh} & 0 \\ 0 & 0 & 0 & J_{h,kh} & J_{h,h}\end{bmatrix}\begin{bmatrix} F_a \\ F_{ak} \\ F_k \\ F_{kh} \\ F_h\end{bmatrix}. \tag{8}$$

In this paper, only non-redundant actuation schemes are studied. Since each leg has three degrees of freedom, only three motors are considered. A proper actuation choice requires that matrix J be not structurally singular. Accordingly, only the following eight architectures have to be considered (see Fig. 1):

- full mono-articular actuation: only one architecture is possible, namely, $\{M_a, M_k, M_h\}$ (architecture 1);
- one bi-articular motor and two mono-articular motors: the bi-articular motor must be completed with one mono-articular motor for the remaining joint. The second mono-articular motor can actuate one of the two joints spanned by the bi-articular motor. Thus, there are four possible architectures: $\{M_a, M_{ak}, M_h\}$, $\{M_{ak}, M_k, M_h\}$, $\{M_a, M_{kh}, M_h\}$, $\{M_a, M_k, M_{kh}\}$ (architectures 3, 6, 4, 2 resp.)
- two bi-articular motors and one mono-articular motor: the two bi-articular motors are necessarily M_{ak}, M_{kh}. The complementary mono-articular motor can be at any of the three joints. Thus there are three possible architectures: $\{M_a, M_{ak}, M_{kh}\}$, $\{M_{ak}, M_k, M_{kh}\}$, $\{M_{ak}, M_{kh}, M_h\}$ (architectures 5, 7, 8, resp.),

With a full mono-articular actuation, matrix J remains diagonal and the design of the robot is easier. In contrast, the introduction of bi-articular motors induces coupling between joints that increases the design difficulty. Thus, architecture 1 will be studied first. The architectures containing bi-articular motors will be considered afterwards.

3. Design problem statement

The joint torque applied by a linear motor does not depend only on the linear motors' features. It also relies on the position of its two attachment points A_j and B_j on the leg, as well as on the joint configuration of the leg. The objective of the design phase, for a given actuation scheme (see Fig. 1) is to determine the position of A_j and B_j. In the preliminary design phase, the assumption that the mass distribution is not affected by the position of the attachment points, implies that the choice of points A_j and B_j affects matrix J but not the dynamic model (1). This allows us to decompose the problem by studying matrix J while the desired motion and corresponding torques are preliminary inputs of the problem. Since the transmission ratio depends on the configuration q of the leg, it is important to consider all movements that the leg has to experience. This will avoid any singularity in the useful range of joints, and exploit the fact that the lever arm varies as a function of the angle.

3.1. Desired trajectories

The first step is to define the tasks to be performed by the robot. In the case of a walking robot, one must define the type of movement that the robot is requested to experience. As an illustration, the robot is requested to walk as well as to perform squat movements (that is, motions from sitting to standing configurations). For the design, it is more important to cover different types of desired movements than to include several movements with similar torque and position requirements. Adding walking movements at different speeds, running, carrying heavy loads, would affect the optimal solution but not the methodology. Two desired movements are considered for the design: a periodic walking and a squat motion. To define the periodic walking, a literature review on human motions [39] allows us to choose a joint motion $t \mapsto q(t)$. This pattern is approximated via a polynomial function for a walking velocity of 2 km/h. The velocity $t \mapsto \dot{q}(t)$ and acceleration $t \mapsto \ddot{q}(t)$ can be deduced and the torque can thus be evaluated according to the dynamic model (1). To avoid dealing with a partition of the contact forces in double support phase, only single support is considered. The behaviour in double support phase is considered via a squat motion defined in [40], for which the two legs have the same motion and the ground force is assumed to be identical on both feet. For these two desired motions, the zero moment point is always inside the sole of the robot since the stance foot is assumed flat on the ground.

Once the two desired motions are defined, the data of one leg are collected into a table composed of time vectors:

$$D(t) = [t, q_a(t), q_k(t), q_h(t), \Gamma_a(t), \Gamma_k(t), \Gamma_h(t)]^\top. \tag{9}$$

The collected data correspond to one stance support, one swing phase and one squat motion. For the concatenation of these motions, t varies from 0 to T where T is the total duration of the motion. Time t is used to associate Γ and q only. Fig. 3 shows torque plots on the hip, knee and ankle against the joint values for the considered motions.

As expected, the maximal torques are observed for stance phases and squat motions. The largest torque appears on the ankle joint for walking and on the knee joint for squat. The rotation range of all joints is limited to approximately 40° during walking. During squat motions, the rotation range is about 100° for the hip, 80° for the knee, and 40° for the ankle. The rotation range is a crucial parameter to avoid singularity when linear motors are used, as it will be discussed in Section 4.1. Note that the ranges of the ankle, knee and hip rotations of a human leg in sagittal plane are a bit higher but do not exceed 155° [41,42].

3.2. Criterion optimized

For a rotary motor, the gear ratio is chosen to handle the trade-off between torque and velocity. In the case of a linear motor, this trade-off is managed by defining suitable motor attachment points. However, for practical and aesthetic reasons, the attachment points will have to be close to the joints. Bounds on the attachment area are deduced from design and bio-inspiration considerations. The set of possible attachments is denoted by S, and will be more precisely defined in the following, see for example Fig. 6. As a result, the transmission ratio remains limited and the most active dimensional constraint is the available force. Consequently, the motors are selected according to the maximum force they have to produce. For the design obtained and the movements expected, we verify *a posteriori* that motor velocities stay always under the limits met in high-power linear motors available on the market. The linear motors used in this study can produce positive and negative forces. For simplicity, each motor force F_j is assumed bounded by the same value F_M: $|F_j| \leq F_M$. The objective is therefore to find the placement of the motor attachment points that minimizes F_M for all the joint configurations and torques belonging to the desired trajectories $D(t)$.

The optimization problem can be stated as follows. For a leg architecture composed of three motors M_1, M_2, M_3 corresponding to one of the eight actuation schemes shown in Fig. 1, find the best attachment points A_1, B_1, A_2, B_2, A_3, B_3 that minimize the maximal forces required at all joints:

$$\mathcal{C}_1 = \min_{(A_1,B_1,A_2,B_2,A_3,B_3)\in S} (\max(|F_1|, |F_2|, |F_3|)) \tag{10}$$

such that

$$\forall t, q_a(t), q_k(t), q_h(t), \Gamma_a(t), \Gamma_k(t), \Gamma_h(t) \in D(t), \quad \begin{bmatrix} \Gamma_a \\ \Gamma_k \\ \Gamma_h \end{bmatrix} = J(q_a, q_k, q_h) \begin{bmatrix} F_1 \\ F_2 \\ F_3 \end{bmatrix} \tag{11}$$

Upon solving the above optimization problem, criterion $\mathcal{C}_1$ provides the value of F_M required to produce the desired motions. This value allows us to choose the motors assuming that the same motors are used for all joints. A more general case can be defined by introducing weights in $\mathcal{C}_1$ as follows:

$$\mathcal{C}_1 = \min_{(A_1,B_1,A_2,B_2,A_3,B_3)\in S} (\max(\alpha_1|F_1|, \alpha_2|F_2|, |F_3|)) \tag{12}$$

where α_1, α_2 are up to the designer if different motors are used.

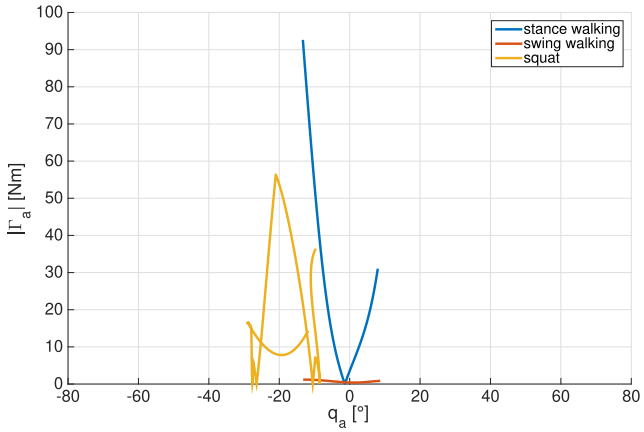

a)

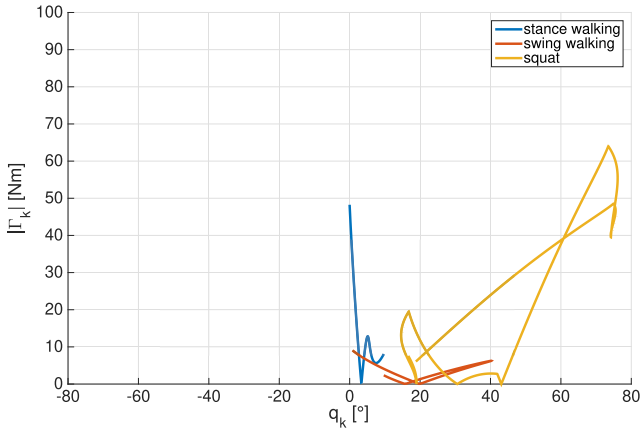

b)

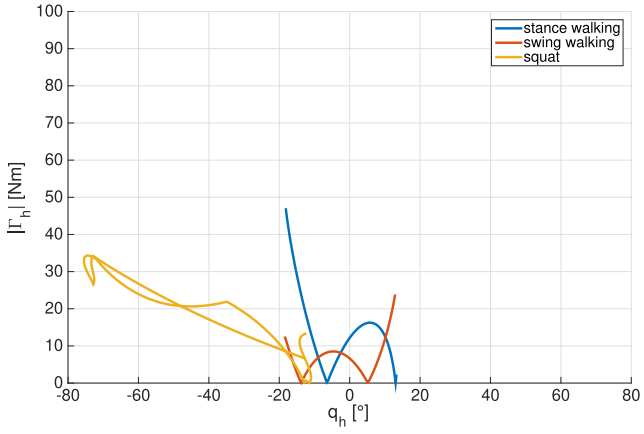

c)

Fig. 3. (a) ankle torque against ankle joint, (b) knee torque against knee joint, (c) hip torque against hip joint.

Since infinitely many optimal designs exist that produce the same criterion $\mathcal{C}_1$, a second criterion $\mathcal{C}_2$ shall be considered, which is the minimization of the integral of the squared norm of F. This allows us to reduce simultaneously the maximal motor forces and the loss of energy by Joule effects in the motors. This criterion is well suited to walking robots that produce periodic motions with null integral of energy when friction is neglected. It may be sensitive to the choice of desired trajectories and especially to the duration of squat and walking trajectories.

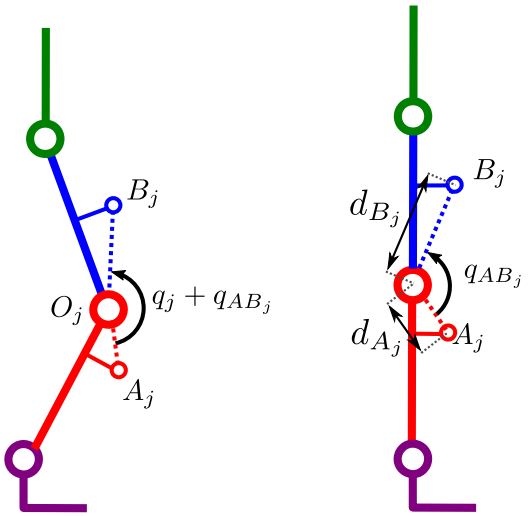

Fig. 4. Notation for a mono-articular actuation, case of the knee.

This second criterion is written as:

$$\mathcal{C}_2 = \min_{(A_1,B_1,A_2,B_2,A_3,B_3)\in S} \int_{t\in D} (F_1^2 + F_2^2 + F_3^2)\mathrm{d}t \tag{13}$$

such that:

$$\forall t, q_a(t), q_k(t), q_h(t), \Gamma_a(t), \Gamma_k(t), \Gamma_h(t) \in D, \quad \begin{bmatrix} \Gamma_a \\ \Gamma_k \\ \Gamma_h \end{bmatrix} = J(q_a, q_k, q_h) \begin{bmatrix} F_1 \\ F_2 \\ F_3 \end{bmatrix} \tag{14}$$

As for criterion $\mathcal{C}_1$, weights can be introduced in criterion $\mathcal{C}_2$.

3.3. Solving the optimization problem

We would like to have more insight into the optimization problem before solving it numerically. To do so, an analytic-heuristic approach is first conducted to obtain an optimal solution of criterion (10). This step allows us to point out several interesting results, such as the existence of singularities pertaining to linear motors, and the necessity to avoid them. The analytic step also instructs on the choice of optimization variables, on their contribution to the optimization problem, and on the great number of acceptable designs. The analytic solving is followed by a numerical optimization. The numerical optimization aims to validate and refine results from the analytic step. It also highlights the limitations of the heuristic approach. On the other hand, the analytic results are used as initial guesses for the numerical optimization. In the numerical approach, the optimization criterion is $\mathcal{C} = \mu\mathcal{C}_1 + \mathcal{C}_2$ with $\mathcal{C}_1$ and $\mathcal{C}_2$ given by (10) and (13), respectively. A large value is used for μ to take into account the difference of magnitude order for the two criteria and to give priority to criterion $\mathcal{C}_1$.

4. Design with three mono-articular motors

The design of a leg with three mono-articular motors is first considered (see architecture 1 in Fig. 1). This case is the simplest, because J is diagonal. Since each motor M_j depends on one unique joint angle q_j and on one unique torque Γ_j, the design of each motor is independent.

4.1. Relationship between motor forces and joint torques

Let us consider one joint j ($j = a$, k, or h) and denote O_j its rotation center in the robot plane. The distance O_jA_j (resp. O_jB_j) is referred to as d_{Aj} (resp. d_{Bj}). The angle $\widehat{A_jO_jB_j}$ is a function of the joint variable q_j. Let us define q_{ABj} as the value of $\widehat{A_jO_jB_j}$ when $q_j = 0$. Notations are detailed in Fig. 4.

The relationship between the motor forces and the joint torques can be written as follows:

$$\Gamma_j = J_{j,j}(q_j)F_j, \tag{15}$$

where $J_{j,j}(q_j) = h_j(q_j)$ is the height of the triangle $A_jO_jB_j$.

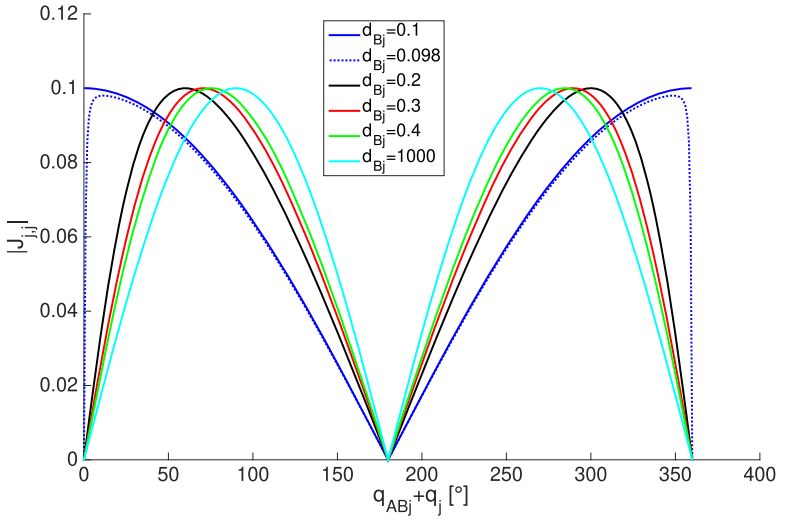

Fig. 5. Evolution of $|J_{j,j}|$ for $d_{Aj} = 0.1$ m for different values of d_{Bj}. For each d_{Bj}, there are two mirrored curves, from 0° to 180° and from 180° to 360°, respectively. Their shapes change when d_{Bj} increases. When d_{Bj} tends to infinity, the associated two curves are symmetric with respect to $q_{ABj} + q_j = 90°$ and $q_{ABj} + q_j = 270°$, respectively.

Overall, the objective of the design optimization is to increase $J_{j,j}(q_j)$ especially for those angle values q_j associated with a high torque Γ_j.

Upon expressing the triangle height $h_j(q_j)$ as a function of its surface using the vector product, the following formula is obtained:

$$J_{j,j}(q_j) = h_j(q_j) = \frac{d_{Aj} d_{Bj} \sin(q_{ABj} + q_j)}{\|\overrightarrow{A_j B_j}\|} \tag{16}$$

where $\|\overrightarrow{A_j B_j}\|$ can be obtained using the cosine rule:

$$\|\overrightarrow{A_j B_j}\|^2 = d_{Aj}^2 + d_{Bj}^2 - 2 d_{Aj} d_{Bj} \cos(q_{ABj} + q_j). \tag{17}$$

The two equations above show us that:

- The scalar $J_{j,j}(q_j)$ can be written with only three parameters d_{Aj}, d_{Bj}, and q_{ABj}, while the definition of the attachment points requires four variables, the coordinates of the attachments points: x_{Aj}, y_{Aj}, x_{Bj}, y_{Bj}. In fact, the overall rotation of triangle $A_j O_j B_j$ does not affect the value of $J_{j,j}(q_j)$.
- Since the term $\sin(q_{ABj} + q_j)$ appears in the numerator, no rotation q_j of range greater than or equal to 180° can be achieved without meeting a singularity where a zero torque is transmitted. This means that linear motors should be used only in situations where singularities can be avoided (otherwise actuation redundancy would be required). Note that the rotation ranges experienced in bipeds satisfy this constraint (see Fig. 3).
- The angle q_{ABj} must be chosen to avoid all singularities. Since a singularity occurs whenever $q_j = -q_{ABj}$, $q_j = 180° - q_{ABj}$ or $q_j = 360° - q_{ABj}$, q_{ABj} should satisfy $0° < q_{ABj} + q_j < 180°$ or $180° < q_{ABj} + q_j < 360°$ for all $q_j \in D$. Upon adding a safety margin of 10°, the condition becomes: q_{ABj} should be such that $10° < q_{ABj} + q_j < 170°$ or $190° < q_{ABj} + q_j < 350°$ for all $q_j \in D$.
- Variables d_{Aj} and d_{Bj} have a symmetrical role in $J_{j,j}(q_j)$. It can be shown that (see Appendix A.1):

$$\max_{0° < q_{ABj} + q_j < 180°} J_{j,j}(q_j) = \min(d_{Aj}, d_{Bj}) \tag{18}$$

and this maximum is reached for

$$q_{ABj} + q_j = \pm \arccos\left(\max\left(\frac{d_{Aj}}{d_{Bj}}, \frac{d_{Bj}}{d_{Aj}}\right)\right). \tag{19}$$

It can be noted that this configuration corresponds to the case where vector $\overrightarrow{A_j B_j}$ is perpendicular to the shortest vector $\overrightarrow{O_j B_j}$ or $\overrightarrow{O_j A_j}$.

- An isometric scaling of d_{Aj} and d_{Bj} by some scalar S scales $J_{j,j}$ by S and thus allows one to produce a torque Γ_j scaled by S, for the same motor.

Fig. 5 depicts the plot of $|J_{j,j}(q_j)|$ against $q_{ABj} + q_j$ for several values of d_{Bj} and for a fixed value of $d_{Aj} = 0.1$. It shows that increasing d_{Bj} so that $d_{Bj} > d_{Aj}$ modifies the shape of the graph of $|J_{j,j}(q_j)|$ and translates the maximum of $|J_{j,j}(q_j)|$

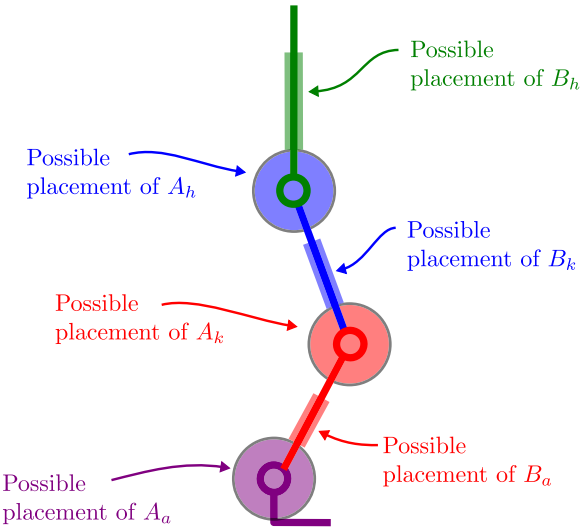

Fig. 6. Possible placement of the attachment points of the three mono-articular linear motors.

but the magnitude of this maximum is not affected. Moreover, $|J_{j,j}(q_j)|$ vanishes whenever $q_{ABj} + q_j = 0°,\ 180°$ and $360°$, independently of d_{Aj} and d_{Bj}. These situations correspond to the singularities where the linear motor cannot transmit any torque.

4.2. Analytic and heuristic design methodology

4.2.1. Limitations on the location of A_j and B_j

For practical designs, A_j and B_j must be located within a predefined possible attachment area. Since a design rule of a humanoid robot requires that the center of mass be close to the trunk [3], the linear motor must be close to the proximal end of the body. The attachment point A_j is linked to the distal body, thus it must be close to the joint center O_j. Accordingly, point A_j is constrained to be in a disc of radius r_{Aj} and centered on O_j. Muscles in human legs are attached to bones. Since it was shown in the previous section that an overall rotation of triangle $A_jO_jB_j$ does not modify the transmission ratio between motor force and joint torque, point B_j can be constrained to be on the axis of the proximal body. These placement areas are illustrated in Fig. 6.

4.2.2. Proposed methodology

The proposed design methodology is based on the following steps:

1. Assign the distance for the most constrained attachment point, namely, A_j. By virtue of Eq. (18), $d_{Aj} = r_{Aj}$ to maximize $J_{j,j}$ for any q_j. For B_j, the distance can be chosen as $d_{Bj} \geq r_{Aj}$. Since the maximum value of $J_{j,j}$ is r_{Aj} (see Eq. (18)), we know that the maximal force F_{Mj} for all motions in D cannot be less than:

$$F_{Mj} = \max_{\Gamma_j \in D} \frac{|\Gamma_j|}{r_{Aj}}. \tag{20}$$

   This means that $\mathcal{C}_1$ is greater or equal to F_{Mj} as defined above. Ideally, $\mathcal{C}_1 = F_{Mj}$ but this is not always possible as shown further.
2. Determine the distance of the second attachment point $d_{Bj} \geq d_{Aj}$ according to the shape of $|\Gamma_j| \in D$ shown in Fig. 3 and based on the shape of $|J_{j,j}|$ given in Fig. 5. Knowing that the minimal motor force is F_{Mj} (Eq. (20)), plot the corresponding torque $F_{Mj}|J_{j,j}|$ for several d_{Bj}. The value of d_{Bj} is determined graphically by playing with the placement of the graph of $F_{Mj}|J_{j,j}|$ along the abscissa axis. The goal is to limit the $|\Gamma_j|$ overshoots over $F_{Mj}|J_{j,j}(q_{ABj} + q_j)|$. The best value of d_{Bj} is selected.
3. Determine q_{ABj}. Changing q_{ABj} allows translating the graph of $F_{Mj}|J_{j,j}|$ along the q_j abscissa axis. Tune the translation so that the singularity is avoided and the overshoots of $|\Gamma_j|$ over $F_{Mj}|J_{j,j}(q_j)|$ are minimized. When $|\Gamma_j| \in D$ has a clear, unique maximum, denote q_{jmax} the value of q_j where this maximum is reached. Since the maximum of $|J_{j,j}(q_j)|$ is

Assign the first attachment point distance $d_{Aj} = r_{Aj}$ and define F_{Mj} with equation (20).

Determine graphically d_{Bj} to minimize the overshoots of $|\Gamma_j(q_j)|$ over $F_{Mj}|J_{j,j}(q_{ABj} + q_j)|$ for a free placement along the abscissa axis.

Determine q_{ABj} so that the singularity is avoided and the overshoots of $|\Gamma_j|$ over $F_{Mj}|J_{j,j}(q_{ABj} + q_j)|$ are minimized.

Fig. 7. Summary of the heuristic method for a mono-articular actuation.

defined in (19), the best value for q_{ABj} is given by:

$$q_{ABj} = \pm \arccos\left(\min\left(\frac{d_{Aj}}{d_{Bj}}, \frac{d_{Bj}}{d_{Aj}}\right)\right) - q_{jmax}. \tag{21}$$

This heuristic methodology is summarized in Fig. 7 and illustrated with an example in the next section.

4.3. Heuristic mono-articular optimal design: case study

The constrained area of the attachment points is chosen as $r_{Aa} = r_{Ak} = r_{Ah} = 0.1$ m. We therefore deduce $d_{Aa} = d_{Ak} = d_{Ah} = 0.1$ m. For the robot to be built, the length of the tibia (resp. of the thigh) is 0.426 m (resp. 0.424 m). Accordingly, 0.1 m $\geq d_{Ba} \geq 0.4$ m, 0.1 m $\geq d_{Bk} \geq 0.4$ m and 0.1 m $\geq d_{Bh} \geq 0.4$ m.

For the ankle, the joint range of q_a is small (see Fig. 3(a)). Thus, we are free to select any value of $d_{Ba} > d_{Aa}$, say $d_{Ba} = 0.2$ m. Moreover, there is a clear, well centered torque peak. In this case, thus, q_{amax} is obtained easily: $q_{amax} = -13.3^\circ$ and q_{ABa} can be defined with Eq. (21). Accordingly, $q_{ABa} = 73.3^\circ$ and $10^\circ < q_{ABa} + q_a < 170^\circ$. Plots of $F_{Ma}J_{a,a}(q_a)$ and $\Gamma_a(q_a) \in D$ against the ankle joint are shown in Fig. 8(a) to illustrate the chosen design.

For the knee, the desired trajectories in D are characterized by a large range of q_k. Besides, Γ_k has two peaks located close to the limits of q_k (see Fig. 3(b)). A value of d_{Bk} close to $d_{Ak} = 0.1$ m is thus appropriate, say $d_{Bk} = 0.11$ m. Since Γ_k has two peaks, q_{kmax} cannot be determined as above. The maximum of $J_{kk}(q_k)$ must be between the two peaks. q_{kmax} is determined graphically as $q_{kmax} = 66^\circ$, while the highest peak of Γ_k is at 73.5°. From (21), $q_{ABk} = -90.6^\circ$. For the resulting design, the maximal force is $F_{Mk} = 665.3$ N. The plots of $F_{Mk}J_{kk}(q_k)$ and $\Gamma_k(q_k) \in D$ are shown in Fig. 8 (middle) to illustrate the chosen design. Small overshoots of $|\Gamma_k(q_k)|$ over $F_{Mk}|J_{k,k}(q_{ABk} + q_k)|$ can be observed and the maximal force required is greater than F_{Mk}.

For the hip, the desired trajectories in D are characterized by a large range of q_h and one high Γ_h peak (see Fig. 3(c)). Moreover, this peak is not centered. Accordingly, we choose $d_{Bh} = 0.13$ m and $190^\circ < q_{ABh} + q_h < 350^\circ$. Then, (21) gives $q_{ABh} = -21.6^\circ$, $F_{Mh} = \max(\frac{\Gamma_h}{d_{Ah}}) = 462.3$ N. The plots of $F_{Mh}J_{hh}(q_h)$ and of $\Gamma_h(q_h) \in D$ are shown in Fig. 8(c)) to illustrate the chosen design.

The corresponding design of the robot showing the attachment points and a simplified representation of the linear motors is also depicted in Fig. 9.

When all attachment points A_a, B_a, A_k, B_k, A_h, B_h are obtained, matrix J can be evaluated and forces F_a, F_k, F_h can be evaluated for all the desired trajectories in D. Next, criteria $\mathcal{C}_1$ and $\mathcal{C}_2$ can be evaluated, either globally or, in this case, for each joint.

4.4. Numerical optimization of the mono-articular design

The optimal design is now conducted numerically with the constraints described in Section 4.3. According to the previous analytic study, two optimization variables d_{Bj} and q_{ABj} are considered for each single joint motor, while d_{Aj} is set to its maximal value defined by the constraint $d_{Aj} = 0.1$ m. Since the optimization of each joint is independent, a separated optimization is conducted for each joint using (15). This allows criterion $\mathcal{C}_1$ in (10) to be taken into account for non-penalizing joints. This criterion provides infinitely many solutions. Additionally, criterion $\mathcal{C}_2$ defined in (13) is added to select a solution minimizing the integral of the square of the motor forces. Accordingly, the compound criterion $\mathcal{C} = \mu\mathcal{C}_1 + \mathcal{C}_2$ is considered, where coefficient μ is set to an arbitrary high value (chosen here as 30,000).

An optimization algorithm based on sequential quadratic programming algorithm is used. Cases $10^\circ < q_{ABk} + q_k < 170^\circ$ and $190^\circ < q_{ABk} + q_k < 350^\circ$ are treated successively and the best solution is chosen. The obtained results are summarized in Table 2 and compared to those of the analytic/heuristic approach.

The numerical optimization algorithm was run with the `fmincon` solver provided by the Matlab©Optimization Toolbox. The optimization takes 28 iterations and around 13 s on a personal computer (2 GHz Intel Core i5) to converge. Note that having a lower bound to the optimal value can help to assess the quality of the numerical solutions found by the

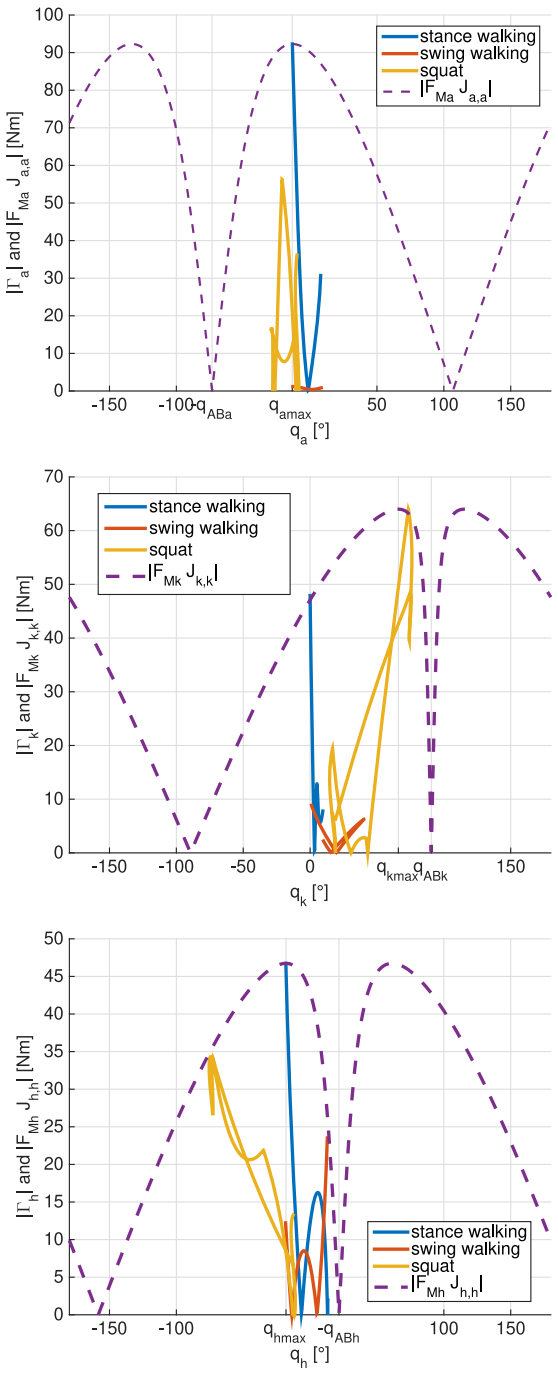

Fig. 8. Heuristic mono-articular design: ankle joint (above), knee joint (middle) and hip joint (below). Plots of $F_{Mj}J_{j,j}(q_j)$ are shown in purple. Plots of $|\Gamma_j|$ coming from Fig. 3 have been added. (For interpretation of the references to color in this figure legend, the reader is referred to the web version of this article.)

optimization solver. In our case, one can determine a lower bound of $\mathcal{C}_1$ for each joint. Indeed, the required force for each joint cannot be smaller than the maximal torque in D divided by the maximal level arm (see Eq. (20)). Since the attachment points of each motor are in a disc of radius 0.1 m, the maximal level arm (see (18) is also 0.1 m. Thus, the lower bounds of $\mathcal{C}_1$ are 922.9 N for the ankle, 639.9 N for the knee and 467.3 N for the ankle, respectively. It can be observed that the computed numerical solution found reaches the lower bound of $\mathcal{C}_1$ for the ankle and the hip. For the knee, $\mathcal{C}_1$ exceeds its lower bound by 0.3% only. This shows that the computed solutions are of excellent quality.

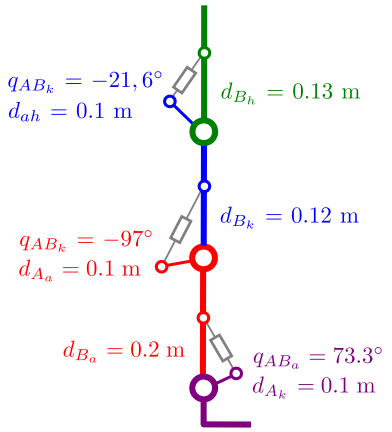

Fig. 9. Optimal design with three mono-articular linear motors.

Table 2
Results of the optimization with the proposed heuristic and numerical approaches.

	Parameters	$\mathcal{C}_1$ N	$\mathcal{C}_2$ 10^5 N^{2}s
Method	Heuristic		
Ankle	$d_{Ba} = 0.2$ m, $q_{ABa} = 73.3°$	922.9	1.63
Knee	$d_{Bk} = 0.11$ m, $q_{ABk} = -90.6°$	651.2	1.66
Hip	$d_{Bh} = 0.13$ m, $q_{ABh} = -21.6°$	467.3	1.32
Total		922.9	4.62
Method	Numeric		
Ankle	$d_{Ba} = 0.17$ m, $q_{ABa} = 66.6°$	922.9	1.63
Knee	$d_{Bk} = 0.105$ m, $q_{ABk} = -86.2°$	642.1	1.63
Hip	$d_{Bh} = 0.14$ m, $q_{ABh} = -25.7°$	467.3	1.31
Total		922.9	4.58

It can be noted that criterion $\mathcal{C}_1$ pertaining to the complete robot is identical in both cases and is large: $\mathcal{C}_1 = 922.9$. It is the ankle joint that is the penalizing joint for the chosen movements. The results of the heuristic and numerical methods are close.

5. Optimization with bi-articular motors

The force produced by a bi-articular motor applies a torque on two joints. When an architecture with one bi-articular motor is considered, two joints and two motors have to be considered together. As a case study, let us consider architecture (M_a, M_{ak}, M_h). Both the ankle joint and the knee joint must be considered together, while the hip joint can be treated alone. For an architecture with two bi-articular motors, the three joints must be considered together. We will show that rewriting Eq. (8) allows us to decouple the relationship between forces and torques.

5.1. Relationship between motor forces and joint torques

The bi-articular motor M_{ak} is treated as an example. The terms $J_{a,ak}$ and $J_{k,ak}$ in Eq. (8) can be written in order to show the relationship between the joint torques Γ_a, Γ_k and the motor force F_{ak}. For more simplicity in the writing, the indices are omitted in the motor attachment points, which are simply written A and B.

As shown in Fig. 10, point A is attached to the distal body (the foot) at a distance d_A from the ankle joint center O_a and with an angle q_A with respect to the vertical. Point B is attached to the proximal body (the thigh) at a distance d_B from the knee joint O_k and with an angle q_B with respect to the thigh axis. Let l denote the distance between O_a and O_k i.e. the length of the tibia.

It can be shown (see appendix (Section A.2)) that:

$$J_{a,ak} = \frac{d_A d_B \sin(q_A - q_a - q_B - q_k) + l d_A \sin(q_A - q_a)}{\|\overrightarrow{AB}\|}, \tag{22}$$

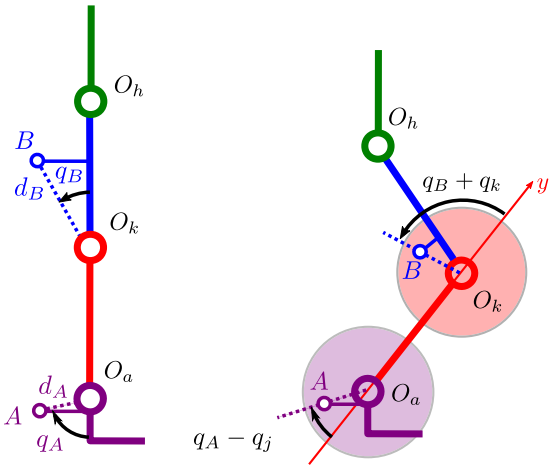

Fig. 10. Position of the attachment points for bi-articular actuation.

$$J_{k,ak} = \frac{d_A d_B \sin(q_A - q_a - q_B - q_k) - l d_B \sin(q_B + q_k)}{\|\overrightarrow{AB}\|}, \tag{23}$$

where:

$$\|\overrightarrow{AB}\| = (d_A^2 + d_B^2 + l^2 + 2 d_A d_B \cos(q_A - q_a - q_B - q_k) + 2 l d_A \cos(q_A - q_a) + 2 l d_B \cos(q_B + q_k))^{1/2}.$$

Term $J_{a,ak}$ (resp. $J_{k,ak}$) is the height of triangle AO_aB (resp. AO_kB).

For the calculation of the motor force, both the ankle joint and the knee joint must be taken into account in Eq. (8). We obtain:

$$\begin{bmatrix} \Gamma_a \\ \Gamma_k \end{bmatrix} = \begin{bmatrix} J_{aa}(q_a) & J_{a,ak}(q_a, q_k) \\ 0 & J_{k,ak}(q_a, q_k) \end{bmatrix} \begin{bmatrix} F_a \\ F_{ak} \end{bmatrix}. \tag{24}$$

This equation will be rewritten in order to decouple the two equations.

For the design at hand (M_a, M_{ak}, M_h), only the bi-articular motor M_{ak} applies a torque on the knee joint. Thus, $J_{k,ak}$ must be different from zero to avoid any singularity. The ratio between $J_{a,ak}$ and $J_{k,ak}$ accounts to the extra torque applied on the ankle joint when a torque on the knee is desired. The ratio r_{ak} can be thus defined as $r_{ak} = \frac{J_{a,ak}}{J_{k,ak}}$:

$$r_{ak} = \frac{d_A}{d_B} \left(\frac{d_B \sin(q_A - q_a - q_B - q_k) + l \sin(q_A - q_a)}{d_A \sin(q_A - q_a - q_B - q_k) - l \sin(q_B + q_k)} \right) \tag{25}$$

Introducing the ratio r_{ak}, the above equation is rewritten as:

$$\begin{bmatrix} \Gamma_a \\ \Gamma_k \end{bmatrix} = \begin{bmatrix} J_{aa}(q_a) & r_{ak}(q_a, q_k) J_{k,ak}(q_a, q_k) \\ 0 & J_{k,ak}(q_a, q_k) \end{bmatrix} \begin{bmatrix} F_a \\ F_{ak} \end{bmatrix}. \tag{26}$$

When the bi-articular motor M_{ak} applies a torque Γ_k on the knee, it also applies a torque $r_{ak}\Gamma_k$ on the ankle. Thus, the torque to be applied by the mono-articular motor M_a is modified as follows:

$$\begin{bmatrix} \Gamma_a - r_{ak}\Gamma_k \\ \Gamma_k \end{bmatrix} = \begin{bmatrix} J_{aa}(q_a) & 0 \\ 0 & J_{k,ak}(q_a, q_k) \end{bmatrix} \begin{bmatrix} F_a \\ F_{ak} \end{bmatrix}. \tag{27}$$

The equations are now decoupled, the physical coupling being included in r_{ak} that depends on q_a, q_k and on design parameters d_A, d_B, q_A, q_B.

5.2. Analytic heuristic design methodology

For the mono-articular motors M_a and M_h, the attachment points are constrained as previously. For the bi-articular motor M_{ak}, the attachment points are constrained to belong in a disc located around the joint axis as illustrated in Fig. 10: $d_A \leq r_A$, $d_B \leq r_B$.

The proposed approach consists in determining the motor attachment points with Eq. (27). It is conducted in three main steps summarized in Fig. 11:

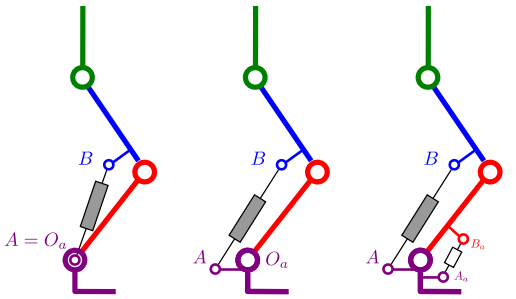

The bi-articular motor M_{ak} is treated as a mono-articular for moving the knee, assuming that A is placed at the ankle joint center O.

Choose the pose of A in order to minimize the maximum of $\Gamma_a - \tilde{r}_{ak}\Gamma_k$ where $\tilde{r}_{ak}$ is an approximate value of r_{ak}

The mono-articular ankle motor is designed to apply the torque $\Gamma_a - r_{ak}\Gamma_k$

Fig. 11. The three steps of the methodology for the design of a bi-articular motor M_{ak} associated to a mono-articular motor M_a.

- In the actuation architecture at hand, the knee is actuated by the bi-articular motor only. Thus, this joint is considered first. A design is proposed by assuming that the distal attachment point A coincides with O_a. This approximation allows us to treat the bi-articular motor as a mono-articular one, i.e. its length varies only with the variation of knee joint q_k. The effect on the design is limited since we have observed that the transmission ratio is strongly affected by the smallest distance from the attachment points to the joint center. Here the limiting factor is d_B and the optimal solution is $d_B = r_B$. As it will be detailed further, only parameters d_B and q_B are involved in this step.
- A second objective of the bi-articular motor is that is contributes positively to the ankle joint. Parameters d_A and q_A are then determined to meet this objective.
- Finally, the parameters of the mono-articular ankle joint are determined.

These three steps are detailed below.

5.2.1. Choice of $\mathrm{d_B}$, $\mathrm{q_B}$

The design of the bi-articular motor is first regarded by focusing on its contribution to the knee joint. The second line of matrix Eq. (27) is thus considered, the objective being to maximize $J_{k,ak}(q_a, q_k)$ at all useful configurations q_a, q_k in order to minimize $|F_{ak}|$ required to apply the desired torque Γ_k in D.

Let us see how $|J_{k,ak}|$, defined by (23), varies as a function of $q_k + q_B$ and $q_a - q_A$. Assume $l = 0.43$ m, $d_A = 0.05$ m and $d_B = 0.1$ m. A contour plot representation in plane $(q_k + q_B,\ q_a - q_A)$ is provided in Fig. 12. It appears that $|J_{k,ak}|$ varies essentially as a function of $q_k + q_B$ and that $|J_{k,ak}|$ never exceeds d_B. This limit on the height of triangle AO_kB can be reached when $\overrightarrow{AB}$ is perpendicular to $\overrightarrow{O_kB}$ if the distance between O_k and A is always greater than d_B.

When the ankle rotates, the attachment point A of the bi-articular motor moves on a circle of radius d_A about O_a. This motion produces few variation of $J_{k,ak}$ as it can be seen in Fig. 12. To simplify the problem, it is thus proposed to assume that the contribution of motor M_{ak} on the knee is equivalent to the contribution of a mono-articular motor with A placed at O_a. This simplification assumes that $d_A = 0$. It is reasonable if d_A is small with respect to the length of the tibia l. Under this simplification, the optimal value of d_B is its maximal value r_B since l is greater than r_B.

This simplification is equivalent to replace Eq. (23) by:

$$J_{k,ak}(q_k) = \frac{d_B l \sin(q_B + q_k)}{\sqrt{d_B^2 + l^2 - 2 d_B l \cos(q_B + q_k)}}. \tag{28}$$

5.2.2. Choice of $\mathrm{d_A}$, $\mathrm{q_A}$

Since the force of the bi-articular motor M_{ak} contributes to the torque of the ankle, the objective of the design is that this force helps the mono-articular motor M_a. Accordingly, r_{ak} is determined in order to minimize $\Gamma_a - r_{ak}(q_a, q_k)\Gamma_k \in D$ at least for its largest value. Thus, the torque to be delivered by the mono-articular motor to the ankle is reduced. In the literature [38], bipeds are designed to obtain an almost constant ratio. In this study, r_{ak} is not assumed constant. In the heuristic approach, the expression of the ratio is simplified. Using (25), and since l is high with respect to d_A and d_B, the following approximate value of r_{ak} is then obtained:

$$r_{ak}(q_a - q_A) \approx -\frac{d_A}{d_B}\frac{\sin(q_a - q_A)}{\sin(q_k + q_B)}. \tag{29}$$

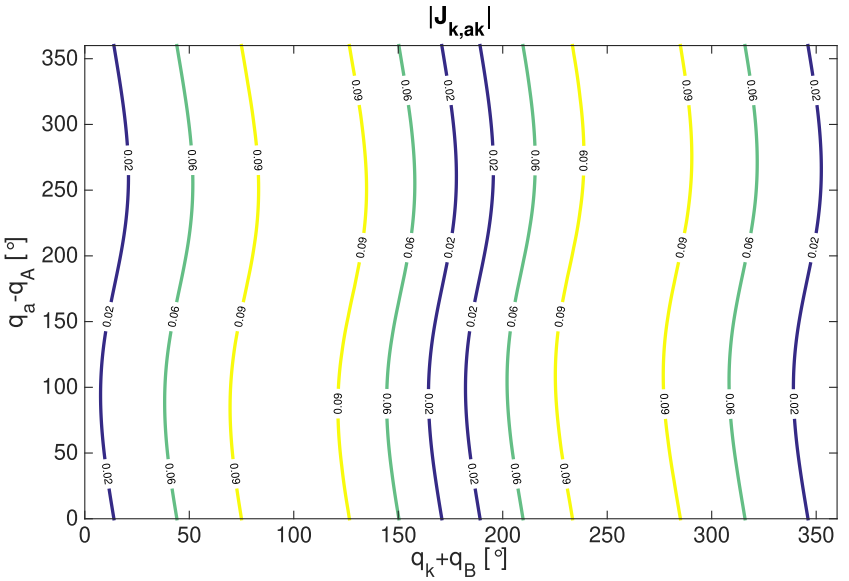

Fig. 12. Contour plot representation of $|J_{k,ak}|$ in the plane $(q_k + q_B,\ q_a - q_A)$ for $l = 0.43$ m, $d_A = 0.05$ m, $d_B = 0.1$ m. $|J_{k,ak}|$ varies essentially as a function of $q_k + q_B$.

Note that $\sin(q_k + q_B)$ must keep the same sign during any motion for a given design, otherwise a singularity would be met. Moreover, a good design will be such that $|\sin(q_k + q_B)|$ is maximized in order to maximize (28). Thus, the ratio r_{ak} can be also approximated by:

$$r_{ak}(q_a - q_A) \approx \tilde{r}_{ak} = -\frac{d_A}{d_B}\frac{\sin(q_a - q_A)}{\text{sgn}(\sin(q_k + q_B))}. \tag{30}$$

Since in the previous step d_B was fixed to $d_B = r_B$, $\frac{d_A}{d_B}$ is bounded as follows:

$$0 < \frac{d_A}{d_B} < \frac{r_A}{r_B}. \tag{31}$$

Consequently, $\tilde{r}_{ak}$ is bounded by:

$$-\frac{r_A}{r_B} < \frac{d_A}{d_B}\sin(q_a - q_A) < \frac{r_A}{r_B}. \tag{32}$$

We now need to determine d_A and q_A to minimize $\Gamma_a - \tilde{r}_{ak}\Gamma_k$. This torque is then plotted in the two extremes cases: $\Gamma_a + \frac{r_A}{r_B}\Gamma_k$ and $\Gamma_a - \frac{r_A}{r_B}\Gamma_k \ \in D$ and the solution that produces the smallest maximum is selected. According to the value of q_a, different ratios may be appropriate and the best solutions for d_A and q_A are chosen knowing the form of $\tilde{r}_{ak}$ (30). An example is shown in the next section.

5.2.3. Design of the associated mono-articular motor

When the bi-articular motor is defined, the exact value of the function $r_{ak}(q_a, q_k)$ can be calculated. The mono-articular motor M_a can then be designed accordingly for the prescribed trajectories in D.

5.3. Heuristic bi-articular optimal design: case study

In Section 4.4, we showed that the ankle is the joint that requires the highest mono-articular motor force. The case where the mono-articular ankle joint is helped by a bi-articular motor is thus detailed in this section. The corresponding actuation scheme is M_a, M_{ak}, M_h. The same constraints on the attachment points as in Section 4.3 are used for the mono-articular motors. For the bi-articular motor, we take $r_A = r_B = 0.1$ m.

For the hip, we use the same mono-articular motor as in Section. 4.3.

For the design of the bi-articular motor M_{ak}, the contribution to the knee torque is treated as a mono-articular motor. Accordingly, $d_B = 0.1$ m, the maximal possible value and $l = 0.426$ m, the length of the tibia. Fig. 13 shows the plots of the knee torques as in Fig. 8, middle. According to this figure, the value of q_B is determined as $q_B = 233°$. Note that this value, when compared to Fig. 8, middle in Section 4.4, is less convenient. The reason is that the number of design parameters is reduced here (l is imposed).

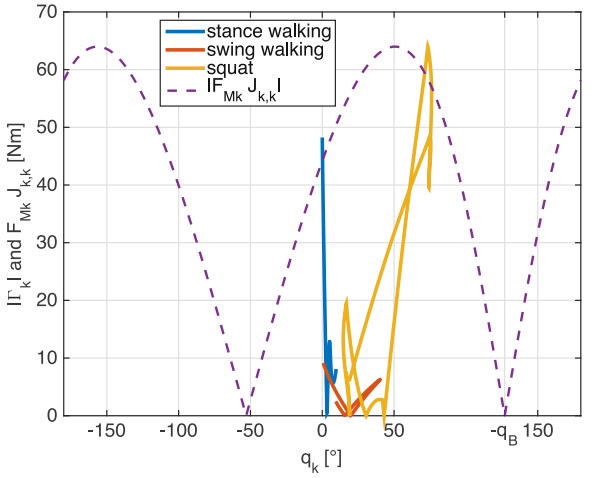

Fig. 13. Case study: determination of q_B for the bi-articular motor.

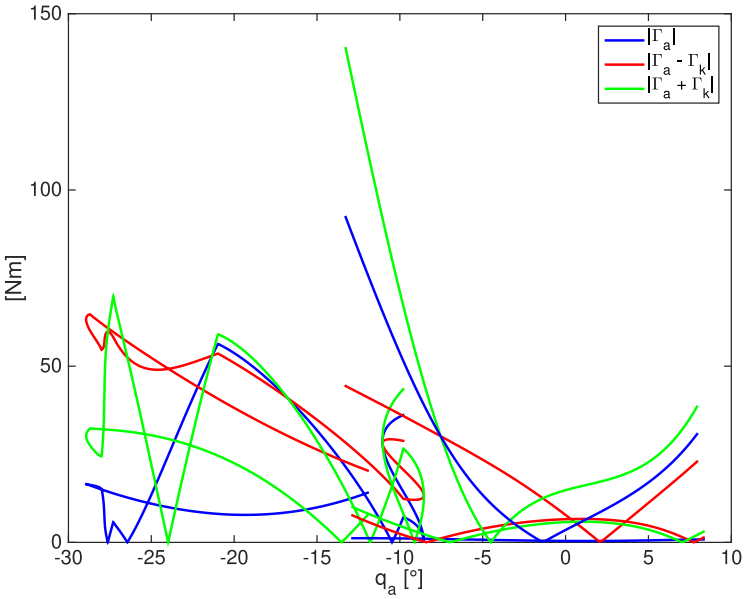

Fig. 14. Torques $|\Gamma_a - \Gamma_k|$ (in red), $|\Gamma_a + \Gamma_k|$ (in green) and $|\Gamma_a|$ (in blue) are plotted against q_a. The maximum of torque at $q_a = -12^\circ$ decreases for $r_{ak} \approx 1$. (For interpretation of the references to color in this figure legend, the reader is referred to the web version of this article.)

The next step is to choose an appropriate ratio r_{ak} in order that motors M_{ak} and M_a cooperate. In accordance with the limits imposed on the placement of the attachment points of M_{ak}: $r_A = r_B = 0.1$ m. The approximate evolution of the ratio $\tilde{r}_{ak}$ is a sinusoidal function of magnitude less than $\frac{r_A}{r_B} = 1$. Thus, the torque to be produced by M_a varies between $\Gamma_a - \Gamma_k$ and $\Gamma_a + \Gamma_k$. Since the torque that M_a can produce depends on q_a, the torques $|\Gamma_a - \Gamma_k|$, $|\Gamma_a + \Gamma_k|$ and $|\Gamma_a|$ are plotted against q_a in Fig. 14, which makes it possible to select an appropriate ratio $\tilde{r}_{ak}$. In order to reduce the maximal torque appearing around $q_a = -12^\circ$, it appears that $\tilde{r}_{ak} \approx 1$ is suitable. Then, thanks to Eq. (30), we obtain $d_A = 0.1$ m and $q_A = 78^\circ$. The corresponding torque $\Gamma_a - \tilde{r}_{ak}\Gamma_k$ is drawn in blue in Fig. 15.

Then, the design of the mono-articular ankle motor is conducted as in Section 4.4 with the torque $\Gamma_{am} = \Gamma_a - r_{ak}\Gamma_k$. Besides, r_{ak} is evaluated here by its real value since d_A, d_B, q_A, q_B are known for the bi-articular motor. The torque Γ_{am} is shown in red in Fig. 15. The variation range of q_a is small, the maximum of Γ_{am} is not centered, thus d_{Ba} is chosen small: $d_{Ba} = 0.11$ m and Eq. (19) yields $q_{ABa} = 53.3^\circ$. This choice is illustrated in Fig. 16.

This optimal solution is given in Table 3. Once the design is finished, the maximal force required for each motor and criterion $\mathcal{C}_2$ are evaluated for all trajectories in D using the complete model (8). Results are added in Table 3. Results for the hip are not presented since they are similar to the mono-actuation design studied in Section 4.

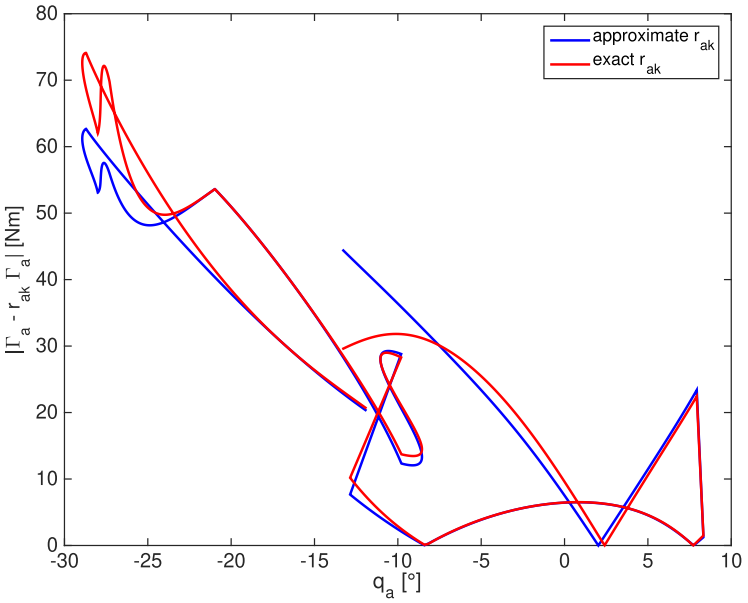

Fig. 15. Torque to be applied by the mono-articular ankle motor: approximate value $\Gamma_a - \tilde{r}_{ak}\Gamma_k$ in blue and real value $\Gamma_a - r_{ak}\Gamma_k$ in red. (For interpretation of the references to color in this figure legend, the reader is referred to the web version of this article.)

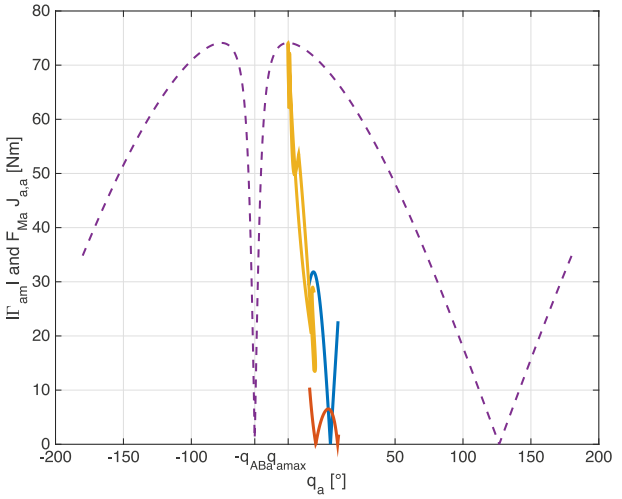

Fig. 16. Case study: design of the mono-articular ankle joint with the torque $\Gamma_a - r_{ak}(q_a, q_k)\Gamma_k$.

5.4. Optimal numerical bi-articular design: case study

The optimal design is now conducted numerically. The constraints on the attachment points are defined in Section 5.2. The results obtained are summarized in Table 3 and compared to the results obtained with the heuristic approach. Note that the optimization problem has many local optima and that the heuristic design is a good initial guess for the optimization problem.

As compared with the three-mono-articular-motor optimal design (Table 2), the results show that the use of a bi-articular motor M_{ak} together with a mono-articular motor M_a for the ankle, allows reducing the maximal force required. Thus, a smaller motor can be used to produce the desired motions. With this design, on the other hand, the integral of the forces to be produced is slightly increased by the use of a bi-articular motor.

As expected, the design obtained with the numerical optimization is better. Indeed, the heuristic method relies on several approximations and the numerical optimization was run with the result of the heuristic approach as an initial guess.

Like for the mono-articular optimal design, we now determine a lower bound for C_1 in order to assess the quality of the computed optimal solutions. Since the attachment points of each motor are in disc of radius 0.1 m, the maximal level arm

Table 3
Optimization results with heuristic and numerical methods for actuation schemes M_a, M_{ak}, M_h.

	Parameters	$\mathcal{C}_1$ N	$\mathcal{C}_2$ 10^5 N ^{2}s
Method	Heuristic		
M_a: Ankle	$d_{Ba} = 0.11$ m, $q_{ABa} = 53.3^\circ$	741	3.06
M_{ak}: Knee	$d_B = 0.1$ m, $q_B = -127^\circ$	776.1	2.02
M_{ak}: Ankle	$d_A = 0.1$ m, $q_A = 78^\circ$		
M_h: Hip	$d_{Bh} = 0.13$ m, $q_{ABh} = -21.6^\circ$	467.3	1.32
Total		776.1	6.4
Method	Numerical		
M_a: Ankle	$d_{Ba} = 0.15$ m, $q_{ABa} = 64.5^\circ$	722.6	1.63
M_{ak}: Knee	$d_B = 0.1$ m, $q_B = -143^\circ$	722.6	1.96
M_{ak}: Ankle	$d_A = 0.03$ m, $q_A = 47^\circ$		
M_h: Hip	$d_{Bh} = 0.14$ m, $q_{ABh} = -25.7^\circ$	467.3	1.31
Total		722.6	4.9

is 0.1 m for both the mono-articular and the bi-articular cases. In any case, the ratio between force and torque is the height of triangle AO_iB, where A and B are the attachment points and O_i the rotation axis. For the knee, since only one motor is involved, the maximal torque in D divided by the maximal level arm, which gives 639.9 N, provides a lower bound for $\mathcal{C}_1$. For the ankle, since two motors are involved, the maximal torque in D divided by the maximal level arm and divided by 2, which gives $\frac{922.9}{2}$ N, provides a lower bound for $\mathcal{C}_1$. Since the two joints are considered simultaneously in the optimization, the optimal value $\mathcal{C}_1$ is necessarily greater than $\max(639.9, \frac{922.9}{2}) = 639.9$ N. The numerical optimization takes 36 iterations and around 14 seconds on a personal computer (2 GHz Intel Core i5).

It is noteworthy that the same maximal motor forces are required for M_{ak} and M_a. This result is consistent with criterion C_1 used for two coupled motors (the optimum is generally reached when the two values are identical). The optimal value obtained by numerical calculation exceeds the minimum value of 13% while the optimal solution obtained by heuristic method exceeds the minimum value of 21%.

6. Comparison of several architectures with three motors

The eight architectures shown in Fig. 1 were optimized following the same approach as in the previous case studies. In order to allow a placement of the motor as close as possible to the trunk, the constraints on the motor attachment points are the following:

- For the distal attachment point, a disc of 0.1 m around the joint is considered.
- For bi-articular motors, a disc of radius 0.1 m around the joint center is considered for the proximal attachment point.
- For mono-articular motors, the proximal attachment point is aligned with the axis of the body at a distance between 0 and 0.4 m to the joint center.

Depending on the architecture considered, there are one, two or three motors acting on a joint and the number of coupled motors in the optimization varies accordingly. For each joint, the minimal force required is the maximal torque in D divided by the maximal level arm (0.1) and by the number of motors acting on the joint (1, 2, or 3). If the joints are coupled by motors, then the maximum of the minimal forces for these joints gives $\mathcal{C}_1$. If the joint is actuated independently, the minimal force for this joint gives $\mathcal{C}_1$. The lower bound of $\mathcal{C}_1$ for each architecture is shown in Fig. 17 with an horizontal black line segment. When compared to the computed optimal solutions, it provides information on the quality of the optimization. It also gives *a priori* information on the design that is best suited to the task. In the case studied, we observe that design 5 may be interesting since the lower bound of $\mathcal{C}_1$ is less than for the other designs.

The optimization was started with the solution provided by the heuristic method. The numerical optimization time is 26 s in average and always less than 50 s. The optimal solutions for the eight architectures are given in Appendix A.3. The results are summarized in Figs 17 and 18 for criteria $\mathcal{C}_1$ and $\mathcal{C}_2$, respectively.

6.1. Best design

As expected, the best design is design 5 : (M_a, M_{ak}, M_{kh}) two bi-articular motors spanning the ankle-knee and the knee - hip, respectively, and a mono articular motor for the ankle (see Fig. 17). This design allows sharing the ankle torque between several motors. For the optimal solution, $\mathcal{C}_1$ exceeds the minimal value by 3.8%. Thus, this design is excellent with respect to this criterion. This result is quite consistent with the study on humans. Indeed, it was shown in [43] that the mono-articular ankle muscle and the bi-articular muscle ankle-knee are very active for walking. It is worth noting that the best design for criterion C_1 (Fig. 17) is also a good design for criterion C_2 (Fig. 18).

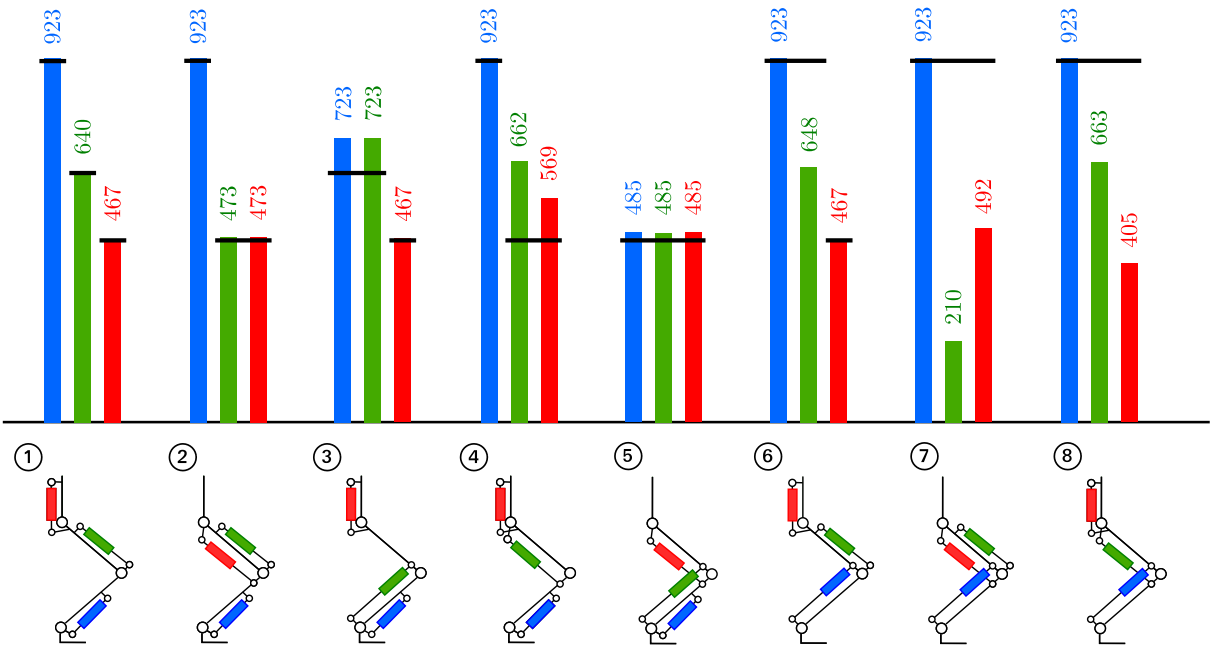

Fig. 17. Maximal force (in N) required for each motor for the eight architectures. Lower bound of C1 for each leg architecture is also shown with a black line. Whenever several joints are coupled (architectures 5, 6,7 and 8), the lower bound of C1 was calculated as the maximum of the lower bounds of the coupled joints, and the lower bound must be compared to the maximum of the required forces. The best architecture with respect to criterion C1 is the design 5, the maximal force required is identical for all motors : 485 N.

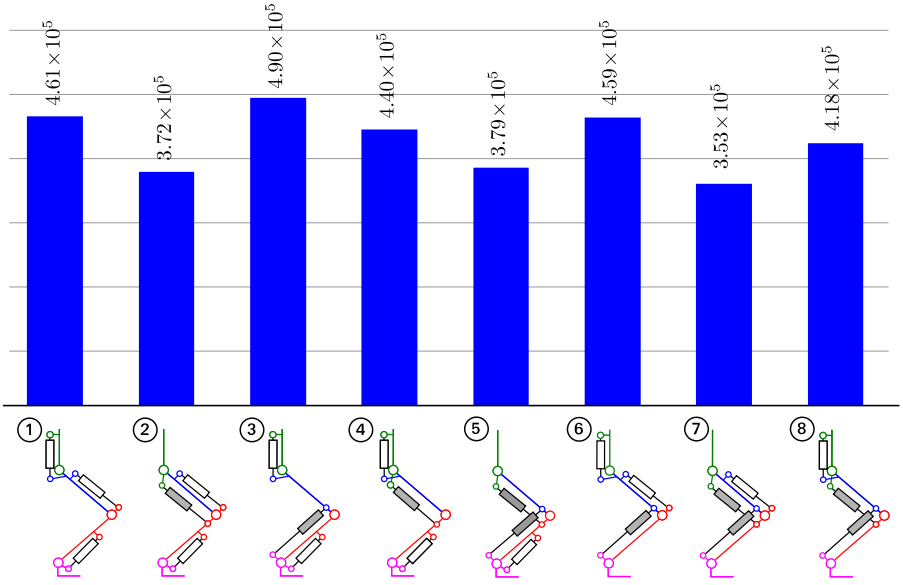

Fig. 18. The integral of force in N^2s is evaluated for the optimal design of each architecture. Architectures 2, 5, 7 are good candidates with respect to this criterion.

The optimal design obtained is shown in Fig. 19. The forces required to produce the achieve configurations and torques in D are shown in Fig. 20 (left) for the optimal design. For comparison purposes, the forces required for the three mono-articular optimal designs depicted in Fig. 9 are shown in Fig. 20 (right).

It can be observed that the force required to move the trunk (F_{kh} or F_h) are of the same order of magnitude (Fig. 20 (bottom)) since only one motor contributes to the torque produced at the hip. For the knee (Fig. 20 (middle)), the maximal force required $max(F_{ak})$ is less than $max(F_k)$ since the bi-articular motor M_{kh} helps M_{ak} with its torque contribution to the knee. For the same reason, the maximal force required $max(F_a)$ for the ankle (Fig. 20 (top)) is lower for the bi-articular

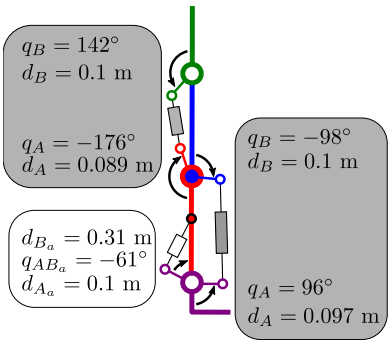

Fig. 19. The optimal design among the eight architectures tested.

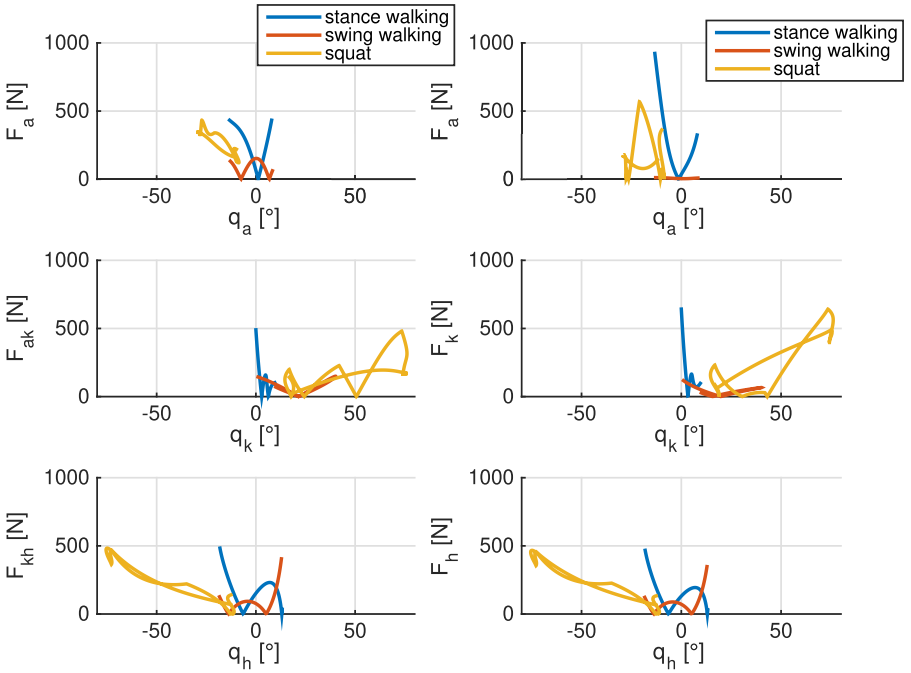

Fig. 20. Forces required for the configurations and torques in D with the optimal design M_a, M_{ak}, M_{kh} (left) or. M_a, M_k, M_h (right).

design since M_{ak} helps M_a with its torque contribution to the ankle. Note, however, that for the swing motion, the force required F_a is higher in the bi-articular design than in the mono-articular one, since the motor force F_a has to counterbalance the torque produced by F_{ak}.

6.2. Discussions

The heuristic approach, although not perfect, allowed us to draw useful conclusions to understand optimal design. It produces an approximate optimal design that allows us to initialize a numerical local optimization algorithm.

The transmission ratio between the force produced by a linear motor and the joint torque is highly dependent on the joint configuration. Moreover, a transmission singularity always occurs in any joint displacement of more than 180°. The trajectories taken into account for the design of our biped can be free of singularities for a good design since the joint ranges remain within 40° and 100° for all joints.

The maximum transmission ratio is limited by the smallest distance of the attachment points to the joint center. This means that if a joint is operated by only one motor, the optimal design yields a motor force equal to the desired maximum torque divided by the maximum lever arm. Trajectories used for the biped design indicate that the maximum torque appears on the ankle joint (92 N.m). With an attachment point area defined by a disc of radius 0.1 m, the motors must provide a force of 920 N. This value can be reduced by accepting a larger attachment point area. Another solution is to have several

motors contributing to the ankle joint. Designs (M_a, M_{ak}, M_h) or (M_a, M_{ak}, M_{kh}) correspond to this case and clearly reduce the required motor forces. Another option would be to accept actuation redundancy.

Disc-shaped attachment point areas were chosen for this study. This choice is consistent with what was shown in the heuristic approach. For mono-articular motors, the optimal solution is the maximum value for the distances d_{Aj}. For bi-articular motors, it is the maximum value for at least one distance d_A or d_B. Other area shapes such as rectangles could be used: the above conclusions would not be changed but they would be more hidden.

For mono-articular joints, the simultaneous rotation of the two attachment points of the motor with respect to the joint axis has not effect on the force required to produce a motion. We have chosen here to place one attachment point on the body axis but other choices would have been possible.

7. Conclusions

Linear motors are becoming more and more efficient, are inherently backdrivable and suitable for bi-articular actuation. In this context, they become interesting to realize compact and bio-inspired bipedal robots. However, the efficiency of linear motors is very sensitive to the placement of their attachment points. The objective of the method presented in this work is to help the designer to place correctly the linear motors in order to produce the expected motions. The first requirement is to avoid singularities that can occur when the axis of the motor meets the joint axis. Accordingly, the methodology proposed to optimize the linear motors attachment points has the following main features:

- since the transmission ratio of a linear motor depends on the joint configurations, a first step is to choose the movements that the biped must be able to perform: joint configurations and joint torques in particular were the input data of the design problem at hand;
- as our objective is to build a human like leg with attachment points close to the structure, the velocity is not a limiting constraint for the motor. The criterion depends on the motor force only;
- contrary to classical design methods, the approach does not necessitate integrating the dynamic model. It is based on the kinematic model relying motor forces and joint torques. Consequently, the calculation burden is reduced.

The methodology is developed in two different ways: an analytic heuristic method and a numerical method.

The analytic (heuristic) method uses two justified approximations: one in the optimization process for mono-articular joints and another in the kinematic equation for bi-articular joints. This method provides a good understanding of the optimal design properties. Practical design rules are deduced and summarized in Section 6.2. This analytic method, in addition to providing useful information, allows obtaining a good initial guess for the numerical optimization. This is of high interest since the optimization problem treated here has many local minima. The analytic approach allows also one to define, based on the limitation of the placement of the attachment points, a lower bound for the required maximal force. Consequently, it allows one to assess the quality of the design obtained. The numerical method is based on the complete and exact formulation of the equations. Accordingly, it provides a refinement of the optimum obtained with the analytical approach.

When the method is defined to obtain the best placement of the motors for a chosen architecture composed of three mono or bi-articular motors, several architectures can be compared. Finally, eight different leg architectures with three motors and combining different numbers of mono-articular and bi-articular motors have been optimized. Results have pointed out the interest of using bi-articular motors to reduce the maximal force required for each motor.

The proposed method provides a preliminary design for a prototype. This preliminary design is based on an assumed mass distribution (here for a robot with a morphology close to a human) chosen independently of the positions of the motors. Once the optimal design is obtained, it will be useful to build a more precise dynamic model that integrates the precise shape of the bodies and a precise description of the motors independently, in order to verify that the selected motors allow performing the desired movements.

A limitation of the current study is the small number of desired movements taken into account for the optimal design. While keeping the same methodology, different results could be obtained by considering a wider range of movements. It would be relevant to repeat this work for a variety of walking trajectories with different step lengths and speeds. We could also consider running trajectories and analyze their influence on the optimal design.

It would be also interesting to better understand the implementation of muscles in humans in order to consider two extensions of this work. One extension is to take into account traction-only motors in groups of two antagonistic muscles. In this case, we could consider an extension of the approach with more parameters accounting for more attachment freedom. Another extension is to take into account actuation redundancy: this extension would be straightforward for the numerical approach.

Declaration of Competing Interest

This is to declare that the authors of our manuscript have no conflict of interest.

Appendix

A1. Appendix: mono-articular case

The variables d_{Aj} and d_{Bj}, have a completely symmetrical role in $J_{jj}(q_j)$. Thus we propose to rewrite $J_{jj}(q_j)$ as function of $d_{ABj} = \min(d_{Aj}, d_{Bj})$ and $r_{ABj} = \max(\frac{d_{Aj}}{d_{Bj}}, \frac{d_{Bj}}{d_{Aj}})$, thus $r_{ABj} \geq 1$. With these notations, one of the distance is d_{Aj}, d_{Bj} is d_{ABj}, while the other is $r_{ABj}d_{ABj}$. The expression becomes

$$J_{jj}(q_j) = \frac{d_{ABj} r_{ABj} \sin(q_{ABj} + q_j)}{\sqrt{1 + r_{ABj}^2 - 2r_{ABj}\cos(q_{ABj} + q_j)}}. \tag{33}$$

The sign of $J_{jj}(q_j)$ is constant for all the $q_j \in D$, since $0^\circ < q_{ABj} + q_j < 180^\circ$ or $180^\circ < q_{ABj} + q_j < 360^\circ$. An increase of d_{ABj} increases the norm of $J_{jj}(q_j)$.

In order to study the extremum of $J_{jj}(q_j)$, its derivative with respect to q_j is calculated. It can be written:

$$\frac{\partial J_{jj}}{dq_j} = d_{ABj} r_{ABj} \frac{-r_{ABj}C_j^2 + (1 + r_{ABj})^2 C_j - r_{ABj}}{(1 + r_{ABj}^2 - 2r_{ABj}C_j)^{(3/2)}} \tag{34}$$

with $C_j = \cos(q_{ABj} + q_j)$. Thus, the extremum is obtained for

$$r_{ABj}C_j^2 - (1 + r_{ABj})^2 C_j + r_{ABj} = 0. \tag{35}$$

The corresponding value of q_j can be obtained as the solution of the second order equation with respect to C_j. Since $r_{ABj} \geq 1$ and $-1 \geq \cos(q_{ABj} + q_j) \geq 1$, the extremum of $J_{jj}(q_j)$ is obtained for:

$$C_j = \cos(q_{ABj} + q_j) = \frac{1}{r_{ABj}} \tag{36}$$

or

$$q_{ABj} + q_j = \pm \arccos\left(\frac{1}{r_{ABj}}\right). \tag{37}$$

The corresponding maximum is

$$\max_{0^\circ < q_{ABj} + q_j < 180^\circ} J_{jj}(q_j) = d_{ABj}. \tag{38}$$

Using the notation d_{Ai}, d_{Bi}, we obtain Eqs. (18) and (19).

A2. Appendix: bi-articular case

The virtual work principle along AB due to F_{ak} can be written as follows:

$$\delta W = F_{ak} \frac{\overrightarrow{AB}}{\|\overrightarrow{AB}\|} \cdot \delta\overrightarrow{AB} \tag{39}$$

or in expanded form:

$$\delta W = F_{ak} \frac{(x_B - x_A)\delta(x_B - x_A) + (y_B - y_A)\delta(y_B - y_A)}{\sqrt{(x_B - x_A)^2 + (y_B - y_A)^2}}, \tag{40}$$

where (x_A, y_A) and (x_B, y_B) are the coordinates of A and B, respectively. First, write the coordinates of point A and B in a frame attached to the intermediate body here the thigh and centered in O_1 (x, directed to the right in the extended leg position, y upwards, on Fig. 10, q_A is negative, q_B positive).

$$\begin{aligned} x_A &= d_A \sin(q_A - q_a), \\ y_A &= -l - d_A \cos(q_A - q_a), \\ x_B &= -d_B \sin(q_B + q_k), \\ y_B &= d_B \cos(q_B + q_k). \end{aligned} \tag{41}$$

We can deduce the coordinates of the vector $\overrightarrow{AB}$:

$$\begin{aligned} x_B - x_A &= -d_B \sin(q_B + q_k) - d_A \sin(q_A - q_a), \\ y_B - y_A &= d_B \cos(q_B + q_k) + l + d_A \cos(q_A - q_h). \end{aligned} \tag{42}$$

We can deduce from this, the norm of the vector $\overrightarrow{AB}$:

$$\|\overrightarrow{AB}\| = (d_A^2 + d_B^2 + l^2 + 2d_A d_B \cos(q_A - q_a - q_B - q_k) + 2ld_A \cos(q_A - q_a) + 2ld_B \cos(q_B + q_k))^{1/2}. \tag{43}$$

we find the expression corresponding to the mono-articular case when $l = 0$ taking into account the fact that $q = \pi + q_A - q_B$.

For a small variation δq_k and δq_h, we will have:

$$\begin{aligned}\delta(x_B - x_A) &= -d_B \cos(q_B + q_k)\delta q_k + d_A \cos(q_A - q_a)\delta q_a.\\ \delta(y_B - y_A) &= -d_B \sin(q_B + q_k)\delta q_k + d_A \sin(q_A - q_a)\delta q_a.\end{aligned} \tag{44}$$

Based on Eq. (2), we can calculate the work of the force:

$$\delta W = F_{ak}\frac{d_A d_B \sin(q_A - q_a - q_B - q_k) - l d_B \sin(q_B + q_k)}{\|\overrightarrow{AB}\|}\delta q_k + F_{ak}\frac{d_A d_B \sin(q_A - q_a - q_B - q_k) + l d_A \sin(q_A - q_a)}{\|\overrightarrow{AB}\|}\delta q_a. \tag{45}$$

We therefore find for the expressions $J_{a,ak}$ and $J_{k,ak}$:

$$J_{a,ak} = \frac{d_A d_B \sin(q_A - q_a - q_B - q_k) - l d_B \sin(q_B + q_k)}{\|\overrightarrow{AB}\|} \tag{46}$$

$$J_{k,ak} = \frac{d_A d_B \sin(q_A - q_a - q_B - q_k) + l d_A \sin(q_A - q_a)}{\|\overrightarrow{AB}\|}. \tag{47}$$

A3. Appendix: the eight optimal designs

The results are summarized in Table 4

Table 4
The eight optimal designs.

	Parameters	$\mathcal{C}_1$ N	$\mathcal{C}_2$ 10^{+5}N ^{2}s
Design 1			
M_a: Ankle	$d_{Ba} = 0.17$ m, $q_{ABa} = 66.6°$	922.9	1.63
M_k: Knee	$d_{Bk} = 0.11$ m, $q_{ABk} = -90.2°$	639.9	1.58
M_h: Hip	$d_{Bh} = 0.14$ m, $q_{ABh} = -25.7°$	467.3	1.31
Total		922.9	4.61
Design 2			
M_a: Ankle	$d_{Ba} = 0.17$ m, $q_{ABa} = 66.6°$	922.9	1.63
M_k: Knee	$d_{Bk} = 0.11$ m, $q_{ABk} = 23.5°$	472.8	0.82
M_{kh}: Knee	$d_A = 0.1$ m, $q_A = 8.4°$		
M_{kh}: Hip	$d_B = 0.1$ m, $q_B = -78.3°$	472.8	1.27
Total		922.9	3.72
Design 3			
M_a: Ankle	$d_{Ba} = 0.15$ m, $q_{ABa} = 64.5°$	722.6	1.63
M_{ak}: Ankle	$d_A = 0.03$ m, $q_A = 47°$		
M_{ak}: Knee	$d_B = 0.1$ m, $q_B = -143°$	722.6	1.96
M_h: Hip	$d_{Bh} = 0.14$ m, $q_{ABh} = -25.7°$	467.3	1.31
Total		722.6	4.9
Design 4			
M_a: Ankle	$d_{Ba} = 0.17$ m, $q_{ABa} = 66.6°$	922.9	1.63
M_{kh}: Knee	$d_A = 0.1$ m, $q_A = 67°$		
M_{kh}: Hip	$d_B = 0.1$ m, $q_B = -42°$	662.2	1.69
M_h: Hip	$d_{Bh} = 0.06$ m, $q_{ABh} = 118°$	569.5	1.07
Total		922.9	4.4
Design 5			
M_a: Ankle	$d_{Ba} = 0.31$ m, $q_{ABa} = -61°$	485	1.63
M_{ak}: Ankle	$d_A = 0.097$ m, $q_A = 96°$		
M_{ak}: Knee	$d_B = 0.1$ m, $q_B = -98°$	485	0.70
M_{kh}: Knee	$d_A = 0.089$ m, $q_A = 184°$		
M_{kh}: Hip	$d_B = 0.1$ m, $q_B = 142°$	485	1.46
Total		485	3.79

(*continued on next page*)

.

Table 4 (*continued*)

	Parameters	$\mathcal{C}_1$ N	$\mathcal{C}_2$ 10^{+5}N ^{2}s
Design 6			
M_{ak}: Ankle	$d_A = 0.1$ m, $q_A = 90.3^\circ$		
M_{ak}: Knee	$d_B = 0.$ m, $q_B = 147^\circ$	922.9	1.66
M_k: Knee	$d_{Bk} = 0.11$ m, $q_{ABk} = -90.2^\circ$	648.9	1.63
M_h: Hip	$d_{Bh} = 0.14$ m, $q_{ABh} = -25.7^\circ$	467.3	1.31
Total		922.9	4.59
Design 7			
M_{ak}: Ankle	$d_A = 0.1$ m, $q_A = 85.4^\circ$		
M_{ak}: Knee	$d_B = 0.046$ m, $q_B = -42^\circ$	922.9	1.63
M_k: Knee	$d_{Bk} = 0.27$ m, $q_{ABk} = -120^\circ$	210.1	0.37
M_{kh}: Knee	$d_A = 0.1$ m, $q_A = -167^\circ$		
M_{kh}: Hip	$d_B = 0.1$ m, $q_B = 142^\circ$	492.1	1.55
Total		922.9	3.53
Design 8			
M_{ak}: Ankle	$d_A = 0.1$ m, $q_A = -117^\circ$		
M_{ak}: Knee	$d_B = 0.$ m, $q_B = -177^\circ$	922.9	1.63
M_{kh}: Knee	$d_A = 0.1$ m, $q_A = -59^\circ$		
M_{kh}: Hip	$d_B = 0.097$ m, $q_B = -39^\circ$	663	1.72
M_h: Hip	$d_{Bh} = 0.142$ m, $q_{ABh} = -26^\circ$	405	0.83
Total		922.9	4.18

References

[1] G. Oort, R. Reinink, S. Stramigioli, New ankle actuation mechanism for humanoid robot, in: Proceedings of the of IFAC World Congress (IFAC'11), 2011, pp. 8082–8088. Milano, Italy, August 28-September

[2] K. Hosoda, T. Takuma, A. Nakamoto, S. Hayashi, Biped robot design powered by antagonistic pneumatic actuators for multi-modal locomotion, Robot. Auton. Syst. 56 (2008) 46–53.

[3] C. Chevallereau, G. Bessonet, G. Abba, Y. Aoustin, Bipedal Robots : Modeling, design and Walking Synthesis, ISTE, Wiley, 2009.

[4] H. Kaminaga, T. Amari, Y. Katayama, J. Ono, Y. Shimoyama, Y. Nakamura, Development of backdrivable hydraulic joint mechanism for knee joint of humanoid robots, in: Proceedings of International Conference on Robotics and Automation, 2009, pp. 1577–1582. Kobe, JAPAN, May 12-17

[5] T. Ishida, A. Takanishi, A robot actuator development with high backdrivability, in: Proceedings of 2006 IEEE Conference on Robotics, Automation and Mechatronics, 2006, doi:10.1109/RAMECH.2006.252631.

[6] P.M. Wensing, A. Wang, S. Seok, D. Otten, J. Lang, S. Kim, Proprioceptive actuator design in the mit cheetah: impact mitigation and high-bandwidth physical interaction for dynamic legged robots, IEEE Trans. Rob. 33 (3) (2017) 509–522.

[7] R. Sellaouti, F.B. Ouezdou, Design and control of a 3dofs parallel actuated mechanism for biped application, Mech. Mach. Theory 40 (12) (2005) 1367–1393.

[8] A. Omer, R. Ghorbani, K. Hashimoto, H. Lim, A. Takanishi, A novel design for adjustable stiffness artificial tendon for the ankle joint of a biped robot: modeling & simulation, Machines MDPI 4 (1) (2016) 2–22.

[9] A. Spröwitz, A. Tuleu, M. Vespignani, M. Ajallooeian, E. Badri, A.J. Ijspeert, Towards dynamic trot gait locomotion: design, control, and experiments with cheetah-cub, a compliant quadruped robot, Int. J. Robot. Res 32 (8) (2013) 932–950, doi:10.1177/0278364913489205.

[10] M.A. Sharbafi, C. Rode, S. Kurowski, D. Scholz, R. Möckel, K. Radkhah, G. Zhao, A.M. Rashty, O. von Stryk, A. Seyfarth, A new biarticular actuator design facilitates control of leg function in *biobiped3*, Bioinspirat. Biomimet. 11 (4) (2016) 1–14.

[11] S. Kalouche, Goat: a legged robot with 3d agility and virtual compliance, in: Proceedings of the 2017 IEEE/RSJ International Conference on Intelligent Robots and Systems (IROS), 2017, pp. 4110–4117.

[12] M.A. Hopkins, D.W. Hong, A. Leonessa, Compliant locomotion using whole-body control and divergent component of motion tracking, in: Proceedings of 2015 IEEE International Conference on Robotics and Automation (ICRA), 2015, pp. 5726–5733.

[13] Z. Li, S. Bai, O. Madsen, W. Chen, J. Zhang, Design, modeling and testing of a compact variable stiffness mechanism for exoskeletons, Mech. Mach. Theory 151 (2020) 03905, doi:10.1016/j.mechmachtheory.2020.103905.

[14] W. Roozing, Z. Ren, N.G. Tsagarakis, An efficient leg with series-parallel and biarticular compliant actuation: design optimization, modeling, and control of the eleg, Int. J. Robot. Res. (2016) 1–17, doi:10.1177/02788364919893762.

[15] T. Bacek, M. Moltedo, C. Rodriguez-Guerrero, J. Geeroms, B. Vanderborght, D. Lefeber, Design and evaluation of a torque-controllable knee joint actuator with adjustable series compliance and parallel elasticity, Mech. Mach. Theory 130 (2018) 71–85, doi:10.1016/j.mechmachtheory.2018.08.014.

[16] G. Kenneally, A. De, D.E. Koditschek, Design principles for a family of direct-drive legged robots, IEEE Robot. Autom. Lett. 1 (2) (2016) 900–907.

[17] K.G. Gim, J. Kim, K. Yamane, Design and fabrication of a bipedal robot using serial-parallel hybrid leg mechanism, in: Proceedings of the IEEE/RSJ International Conference on Intelligent Robots and Systems (IROS), 2018. Madrid, Spain, October 1-5.

[18] S. Seok, A. Wang, M.Y. Chuah, D.J. Hyun, J. Lee, D.M. Otten, Design principles for energy-efficient legged locomotion and implementation on the mit cheetah robot, IEEE/ASME Trans. Mechantron. 20 (2) (2015) 924–933.

[19] A. Rosendo, S. Nakatsu, K. Narioka, et al., Pneupard: a biomimetic musculoskeletal approach for a feline-inspired quadruped robot, in: Proceedings of 2013 IEEE/RSJ International Conference on Intelligent Robots and Systems, 2013, pp. 1452–1457.

[20] M. Raibert, K. Blankespoor, G. Nelson, R. Playter, BigDog, the Rough-Terrain Quadruped Robot, in: IFAC Proceedings Volumes, 41, 2008, pp. 10822–10825, doi:10.3182/20080706-5-KR-1001.01833. 17th IFAC World Congress.

[21] M. Johnson, B. Shrewsbury, S. Bertrand, T. Wu, D. Duran, M. Floyd, P. Abeles, D. Stephen, N. Mertins, A. Lesman, J. Carff, W. Rifenburgh, P. Kaveti, W. Straatman, J. Smith, M. Griffioen, B. Layton, T. de Boer, T. Koolen, P. Neuhaus, J. Pratt, Team IHMC's lessons learned from the DARPA robotics challenge trials, J. Field Robot. 32 (2) (2015) 192–208, doi:10.1002/rob.21571.

[22] P. Jakubik, An autonomous biped-concept and design, in: Proceedings of International Conference on Informatics in Control Automation and Robotics (ICINCO), 2012, pp. 167–176. Rome, Italy, July 28–31

[23] J.L. Peralta, T. Ylikorpi, K. Gulzar, P. Jakubik, A. Halme, Novel design of biped robot based on linear induction motors, in: Proceedings of 2009 IEEE/RAS International Conference on Humanoid robots Intelligent Robots and Systems, 2009, pp. 34–39. Paris, France, 7–10 Dec.
[24] C. Iancu, M. Ceccarelli, E.C. Lovasz, Design and lab tests of a scaled leg exoskeleton with electric actuators, in: Ferraresi Carlo, Quaglia Giuseppe (Eds.), Advances in Service and Industrial Robotics, Springer International Publishing, Cham, 2018, pp. 719–726.
[25] M. Ceccarelli, D. Cafolla, M. Russo, G. Carbone, LARM bot humanoid design towards a prototype, MOJ Appl. Biol. Biomech. 1 (2) (2017).
[26] M. Russo, S. Herrero, O. Altuzarra, M. Ceccarelli, Kinematic analysis and multi-objective optimization of a 3-UPR parallel mechanism for a robotic leg, Mech. Mach. Theory 120 (2018) 192–202, doi:10.1016/j.mechmachtheory.2017.10.004.
[27] C. Marco, R. Matteo, in: Parallel Mechanism Designs for Humanoid Robots", booktitle="Robotics and Mechatronics, Springer International Publishing, Cham, 2020, pp. 255–264.
[28] B. Na, H. Choi, K. Kong, Design of a direct-driven linear actuator for a high-speed quadruped robot, cheetaroid-i, IEEE/ASME Trans. Mechantron. 20 (3) (2015) 1117–1129.
[29] R. Hartramph, E. Veit, H. Scheurenbrand, Linearantrieb, Patent #WO2000031421A1. WIPO (PCT)(2000).
[30] C.A.M. Doorenbosch, G.J. van Ingen Schenau, The role of mono- and bi-articular muscles during contact control leg tasks in man, Hum. Mov. Sci 14 (1995) 279–300.
[31] S. Rasmussen, A.K. Chan, G.E. Goslow, The cat step cycle, electromyographic patters for hindlimb muscles during posture and unrestrained locomotion, J. Morphol. 155 (1978) 253–270.
[32] C.M. Chanaud, J.M. Macpherson, Functionally complex muscles of the cat hindlimb. iii. differential activation within biceps femoris during postural perturbations, Exp. Brain Res. 85 (1991) 271–280.
[33] A.V. Voronov, The roles of monoarticular and biarticular muscles of the lower limbs in terrestrial locomotion, Hum. Physio. 30 (4) (2009) 476–484.
[34] J.B.J. Smeets, Bi-articular muscles and the accuracy of motor control, Hum. Mov. Sci. 13 (1994) 587–600.
[35] K. Junius, M. Moltedo, P. Cherelle, C. Rodriguez-Guerrero, B. Vanderborght, D. Lefeber, Biarticular elements as a contributor to energy efficiency: biomechanical review and application in bio-inspired robotics, Bioinspir. Biomimet. 12 (061001) (2017).
[36] S. Ha, . Coros, A. Alspach, J. Kim, K. Yamane, Computational co-optimization of design parameters and motion trajectories for robotic systems, Int. J. Robot. Res. 37 (13–14) (2018) 1521–1536.
[37] D.A. Winter, Biomechanics and Motor Control of Human Movement, John Wiley and Sons, 2009.
[38] A. Nejadfard, S. Schütz, K. Mianowski, P. Vonwirth, K. Berns, Moment Arm Analysis of the Biarticular Actuators in Compliant Robotic Leg Carl., Springer, Cham, 2018.
[39] J. Perry, Kinesiology of lower extremity bracing, Clin. Orthop. Relat. Res. 102 (18–31) (1974) 100–115.
[40] O. Bordron, C. Huneau, E.L. Carpentier, Y. Aoustin, Joint torque estimation during a squat motion, in: Proceedings of CFM 2019, Twenty-forth Congrès Français de Mécanique,CFM, 2019. Brest, France, August 26–30
[41] J. Buckwalter, T. Einhorn, S. Simon, Orthopaedic Basic Science: Biology and Biomechanics of the Musculoskeletal System, American Academy of Orthopaedic Surgeons, Rosemont, IL, 2000.
[42] W. Jahn, Musculoskeletal examination – range of motion, J. Canad. Chiropr. Assoc. 23 (2) (1979) 51–60.
[43] T. Zielinska, J. Wang, W. Ge, l. Lyu, Comparative study of muscles effort during gait phases for multi-muscle humanoids, in: Proceedings of Twelfth International Workshop on Robot Motion and Control, 2019. Poland, July 8–10